Influence of Precipitation Assimilation on a Regional Climate Model's Surface Water and Energy Budgets

ANA M. B. NUNES AND JOHN O. ROADS

Experimental Climate Prediction Center, Climate Research Division, Scripps Institution of Oceanography, University of California, San Diego, La Jolla, California

(Manuscript received 5 October 2006, in final form 3 January 2007)

ABSTRACT

Initialization of the moisture profiles has been used to overcome the imbalance between analysis schemes and prediction models that generates the so-called spinup problem seen in the hydrological fields. Here precipitation assimilation through moisture adjustment has been proposed as a technique to reduce this problem in regional climate simulations by adjusting the specific humidity according to 3-hourly North American Regional Reanalysis rain rates during two simulated years: 1988 and 1993. A control regional simulation provided the initial condition fields for both simulations. The precipitation assimilation simulation was then compared to the control regional climate simulation, reanalyses, and observations to determine whether assimilation of precipitation had a positive influence on modeled surface water and energy budget terms. In general, rainfall assimilation improved the regional model surface water and energy budget terms over the conterminous United States. Precipitation and runoff correlated better than the control and the global reanalysis fields to the regional reanalysis and available observations. Upward shortwave and downward short- and longwave radiation fluxes had regional seasonal cycles closer to the observed values than the control, and the near-surface temperature anomalies were also improved.

1. Introduction

Many studies have focused on the adjustment of moisture and divergence analyses (e.g., Krishnamurti et al. 1984, 1988, 1991; Donner 1988; Heckley et al. 1990; Puri and Miller 1990; Puri and Davidson 1992; Aonashi 1993; Kasahara et al. 1994; Manobianco et al. 1994; Yap 1995; Treadon 1996) in order to improve precipitation forecasts. Some of these studies have used observed rain rates to directly adjust the moisture and diabatic heating profiles to initialize global and regional models. A few studies have incorporated the precipitation information via a one-dimensional variational data assimilation system, for example, Fillion and Errico (1997) and Marècal and Mahfouf (2000). Hou et al. (2000) defined a 1 + 1D assimilation procedure that consists of a time integration of a simplified column version of the atmospheric general circulation model with full physics. Others have employed even more sophisticated and computationally expensive four-dimensional variational data assimilation systems, for example, Županski and Mesinger (1995), Zou and Kuo (1996), and Tsuyuki (1997). The variational approach used by these data assimilation systems basically consists of minimizing the difference between observations and model forecasts by using a version of the forecast model and its adjoint (a conjugate transpose of the model). However, the inversion of the nonlinear processes such as physical parameterizations in an adjoint model continues to remain a challenging problem.

A more simplified approach to the precipitation assimilation (PA) in atmospheric models is to nudge latent heat rates. This procedure was used by the National Centers for Environmental Prediction (NCEP) North American Regional Reanalysis (NARR; Mesinger et al. 2006) to generate a realistic hydroclimatology. Similarly, Nunes and Cocke (2004) and Nunes and Roads (2005) assimilated precipitation by nudging moisture profiles, mainly because the uncertainties in the humidity fields are much larger than in the temperature (see also Puri and Davidson 1992; Hou et al. 2000; Falkovich et al. 2000).

This PA methodology not only improves atmo-

Corresponding author address: Ana M. B. Nunes, Climate Research Division, Scripps Institution of Oceanography, University of California, San Diego, La Jolla, CA 92093-0224.
E-mail: anunes@ucsd.edu

DOI: 10.1175/JHM615.1

© 2007 American Meteorological Society

Unauthenticated | Downloaded 04/29/25 09:21 AM UTC

spheric characteristics but also improves the surface hydrology and may eventually prove to be superior to the uncoupled methodology used for the Global Soil Wetness Project (GSWP; Dirmeyer et al. 1999), the Global Land Data Assimilation System (GLDAS; Rodell et al. 2004), and the North American Land Data Assimilation System (NLDAS; Mitchell et al. 2004). PA also differs from a previous attempt by the NCEP–Department of Energy (DOE) Atmospheric Model Intercomparison Project (AMIP-II) reanalysis (R-2; Kanamitsu et al. 2002) to use the difference between model precipitation and a 5-day "observed" precipitation mean from the Climate Prediction Center (CPC) Merged Analysis of Precipitation (CMAP) based on the Xie and Arkin (1997) precipitation data to correct soil moisture. In particular, PA may eventually provide some advantage on account of the continuous interaction between the atmospheric and the land surface models.

We examine here a climate analysis of the coupled land surface scheme response to this model-adjusted precipitation, focusing initially on the impact on the surface water budget terms. Because the continuous assimilation of the precipitation produces changes in the surface radiation fluxes by modifying the surface albedo and cloud distribution, which is directly related to the changes in the moisture profiles produced by the assimilation scheme, we also compare the surface radiation terms of all simulations to the Global Energy and Water Cycle Experiment (GEWEX) Surface Radiation Budget (SRB) datasets.

In section 2 we describe the precipitation assimilation procedure, the regional model principal features, the initial and boundary conditions, and datasets used by the assimilation procedure, and we evaluate all simulations. In section 3, the experiment results as well as some of the characteristics of the surface water and energy budget terms are discussed. Section 4 presents some concluding remarks.

2. Methodology

a. Precipitation assimilation scheme

Our precipitation assimilation procedure was influenced by a moisture initialization procedure described in Puri and Miller (1990), which indirectly modified the diabatic heating through changes in the humidity profiles. Falkovich et al. (2000) also modifies specific humidity, changing it in proportion to the difference between the model and observed precipitation in the lower troposphere to trigger the convection in a simplified Arakawa–Schubert scheme.

Here, in order to bring the model's precipitation closer to the observed average values, changes were introduced in the specific humidity vertical profiles, mainly in the lower troposphere, taking into account the difference between "observed" and predicted rain rates as given by

$$q_k^m = q_k + \frac{g}{p_s \Delta\sigma_k} \frac{2l}{N(N+1)} \Delta R \tau. \quad (1)$$

Here q_k is the specific humidity predicted by the model in a k layer and q_k^m is the specific humidity modified by the procedure; g is the gravity, p_s is the surface pressure, and $\Delta\sigma_k$ is the layer thickness. The difference between the "observed" and predicted vertically integrated rain rates interpolated to the model's time step in millimeters per second is ΔR, and τ is the adjustment time, which depends on a vertical scale. For a deep vertical layer the convective adjustment time scale, approximately 30 min, is assumed, which allows faster scheme convergence, and for a shallow layer approximately 4 min is used, which is equivalent to the model's leapfrog time differencing. The total number of k layers over which the specific humidity was modified is represented by N. In the absence of model rain, the humidity was modified beginning ($l = l$, $k = k_{\text{top}}$) from an arbitrary upper humidity level to the top of the surface layer ($l = N$, $k = k_{\text{bottom}}$), where $N = k_{\text{top}} - k_{\text{bottom}} + 1$. When model rain is present only those model layers in which model precipitation is occurring have the humidity modified by the above scheme. The k (and l), and the total N can thus change every model's time step. Note that the specific humidity profile does not become linear; only the precipitation difference is linearly distributed. We still suspect that other humidity correction profiles will eventually provide further improvements, especially for climatological simulations.

The humidity modification is presumably dependent in part upon the model cumulus convection scheme. In that regard, assuming the cumulus convection parameterization needed to be modified the most by the PA procedure, a threshold was chosen for the moisture adjustment; the correction only took place when either "observed" or predicted rain rates were greater than 2.5 mm day^{-1}. It should be noted that the cumulus and large-scale parameterizations determined the latent heat release after the humidity adjustment was imposed.

Although this climatological simulation effort was initially focused on improving the precipitation, we knew that our many assumptions about the vertical distribution could lead to a change in cloud cover, which could, in turn, affect the surface radiation fluxes. These surface radiation changes, which we believe were also

Unauthenticated | Downloaded 04/29/25 09:21 AM UTC

beneficial to the model simulation, will be discussed in section 3c.

b. Model

The version of the Experimental Climate Prediction Center (ECPC)-Regional Spectral Model (RSM; Juang and Kanamitsu 1994) used here is a primitive equation model, with almost identical physics to the driving R-2 Global Spectral Model. In particular, the version of the ECPC-RSM used here has an updated Oregon State University land surface model (OSU LSM; Mahrt and Pan 1984; Pan and Mahrt 1987) with an increased number of vegetation types (OSU2) and two soil layers. The Richards' equation is used to predict the soil moisture profiles. The evaporation takes place from the soil layer top level. Runoff occurs when soil moisture exceeds a determined maximum value (0.47). Details about this version of the land surface scheme are described in Kanamitsu and Mo (2003). Relaxed Arakawa–Schubert (RAS; Moorthi and Suarez 1992) was the cumulus convection parameterization used for the RSM simulations. The shortwave and longwave radiation schemes come from Chou (1992) and Chou and Suarez (1994), respectively. The cloud scheme comes from Slingo (1987). The ECPC-RSM in this study had a horizontal resolution of about 60 km and 28 vertical layers. A Mercator projection was used for the regional grid. The model's orography was constructed from 8-min-resolution orography. The ECPC-RSM boundary conditions are updated every 6 h by the R-2 described below.

c. Datasets

1) Initial and boundary conditions

R-2 (Kanamitsu et al. 2002) is an updated version of the NCEP–National Center for Atmospheric Research (NCAR) reanalysis 1 (R-1; Kalnay et al. 1996; Kistler et al. 2001). R-2 uses a simplified version of the OSU LSM (OSU1) with two soil layers (0–10 and 10–200 cm) as well as in the regional model. In R-2, the observed 5-day mean precipitation based on rain gauge and satellite observations is compared to the model precipitation in order to adjust the soil moisture of the soil top layer. Simplified Arakawa–Schubert (SAS; Pan and Wu 1994) is the cumulus parameterization scheme used by R-2. The cloud parameterization is based on the Campana et al. (1994) scheme. The shortwave radiation scheme comes from Chou (1992) and Chou and Lee (1996), and another one of the improvements from R-1 is that the radiation computations are done on the full Gaussian grid to avoid subsequent interpolation. Similar to R-1, R-2 has a triangular spectral truncation of 62 waves, corresponding to a horizontal resolution of about 210 km at the equator, and 28 vertical layers. R-2 also uses the reanalysis data assimilation system that is described in Kalnay et al. (1996). This system is a three-dimensional variational data assimilation (3DVAR) analysis scheme, where the prognostic variables are assimilated.

2) Evaluation datasets

(i) The North American Regional Reanalysis

The NARR fields (Mesinger et al. 2006) provide a basic evaluation dataset for these experiments and also provide the rain rates used by the PA scheme. NARR is based on the 45-layer/32-km-resolution Eta Model (Mesinger et al. 1988) and its 3DVAR Data Assimilation System (EDAS). The Eta Model convection scheme is the Betts–Miller–Janjić and both boundary layer and convection physics are described in Janjić (1990, 1994). The NARR system also used a cloud microphysics model developed by Zhao et al. (1997). An updated version of the four-layer Noah land surface model (Mitchell et al. 2004) is coupled to the NARR atmospheric model. Among the most important improvements is the direct assimilation of radiances, as well as hourly precipitation (Lin et al. 1999) through diabatic heating profiles adjustments. NARR also uses lateral boundary conditions from R-2. The precipitation dataset used by NARR comes from different sources, including the gauge-only CPC daily precipitation analyses disaggregated into hourly analyses over the contiguous United States, Mexico, and Canada; CMAP; and CPC Morphing Technique (CMORPH) over southern portions of the oceans from January 2003. Over the contiguous United States, the precipitation daily analysis used is 1/8° analysis, which is an inverse square-distance weighting scheme with an orography enhancement technique; Parameter-elevation Regression on Independent Slopes Model (PRISM; Daly et al. 1994) is also applied. This high spatial daily precipitation analysis is then disaggregated to hourly values by employing temporal weights obtained from a coarser-scale 2.5° hourly precipitation analysis. As described in Mesinger et al. (2006), NARR precipitation fields are very close to the precipitation analyses used as input. For this reason and also because NARR provides 3-hourly precipitation outputs, the PA scheme used by the RSM in this study assimilated the 3-hourly NARR rain rates.

(ii) The Surface Radiation Budget Project

The National Aeronautics and Space Administration (NASA) World Climate Research Program (WCRP)/

Unauthenticated | Downloaded 04/29/25 09:21 AM UTC

GEWEX SRB Project developed a 12-yr surface shortwave (SW) and longwave (LW) flux dataset, based on satellite observations. The SRB monthly averages come from the NASA Langley Atmospheric Sciences Data Center (ASDC) on a regular global grid at 1° resolution, and were available to us from July 1983 to October 1995 at the NASA Langley Web page. (More information is available online at http://eosweb.larc.nasa.gov.) The SW and LW fluxes are derived using Pinker and Laszlo (1992) and Fu et al. (1997) algorithms, respectively. The SW models used clear-sky top-of-atmosphere albedo from the Earth Radiation Budget Experiment (ERBE). The cloud properties were taken from the International Satellite Cloud Climatology Project (ISCCP) DX data. The Goddard Earth Observing System-1 (GEOS-1) data assimilation product provided the necessary meteorological profiles. The SW and LW fluxes are originally on a 3-hourly temporal resolution and then averaged into monthly averages. According to the data documentation, the GEWEX/SRB monthly average fluxes were compared with corresponding ground-measured fluxes over the period of 4 yr (1992–95) from a number of sites of the Baseline Surface Radiation Network (BSRN). The mean bias of the SRB fluxes was found within the BSRN uncertainties for that period, which were ± 3–5 W m^{-2} for the LW fluxes, and ± 5–15 W m^{-2} for the SW fluxes. The SRB monthly average surface radiation fluxes used for our study came from release 2 for the SW fluxes, and release 2.1 for the LW fluxes.

(iii) Higgins's precipitation data

Daily rain rates used for the evaluation here are available on a 0.25° resolution grid (Higgins et al. 2000) over the domain 20°–60°N, 140°–60°W. The basic data for this daily precipitation analysis are the CPC Cooperative dataset based on the 24-h "first order" World Meteorological Organization (WMO) sites and the 24-h precipitation reports from the River Forecast Centers. This unified rain gauge dataset is available from 1948 to present.

(iv) The University of New Hampshire runoff datasets

The University of New Hampshire (UNH) Institute for the study of Earth, Ocean, and Space (EOS) provided the 0.5° resolution global runoff dataset used in this study; this dataset was available from January 1950 to December 2000 (courtesy of E. Douglas). These composite runoff fields result from combining river discharge information, which is collected and archived globally by the WMO's Global Runoff Data Centre (GRDC), with climate-driven water balance model outputs. Information about the UNH runoff monthly mean dataset can be found in Fekete et al. (2002).

(v) The Climatic Research Unit temperature datasets

These datasets consist of land-based temperature anomalies, obtained from the base period 1961–90, on a $5° \times 5°$ grid box and available from the Climatic Research Unit (CRU) land station temperature database. This study used revision 2, which comprised 5159 station records, of which nearly 81% had sufficient data over the base period to produce the averages, and develop the temperature anomalies for the period of 1851 to 2001 for the land areas over the world. Over the contiguous United States the temporal and spatial coverage have been updated, merging new datasets with global coverage of long climatic time series. A detailed explanation about the CRU land-based air temperature anomalies (CRUTEM2) can be found in Jones and Moberg (2003).

3. Experiment design and results

Figure 1 shows the simulation domain that also includes the Caribbean Sea, Mexico, and the southern part of Canada. The model domain was originally chosen as part of the Project to Intercompare Regional Climate Simulations (PIRCS; Takle et al. 1999) experiment 1c.

A regional control simulation was carried out over the chosen domain from 1 July 1986 to 31 December 1996; precipitation assimilation was not applied for this control experiment. Two other regional simulations assimilating the 3-hourly NARR rain rates were then performed for 1988 and 1993, using the control simulation initial conditions at 0000 UTC 1 January of both years. Hereafter, these regional experiments will be referred to as PA and Control in order to designate the experiments with and without precipitation assimilation, respectively. In all results shown below, the global and regional reanalyses as well as the validation datasets were interpolated to the RSM output grid.

Figure 1 shows the regional precipitation average of 1988 and 1993 for winter [January–March (JFM)], spring [April–June (AMJ)], summer [July–September (JAS)], and fall [October–December (OND)] over the experiment domain for PA, Control, and NARR. NARR provided the precipitation input for the PA simulations. Assimilation of precipitation does not occur in the southern domain boundary, because the

Unauthenticated | Downloaded 04/29/25 09:21 AM UTC

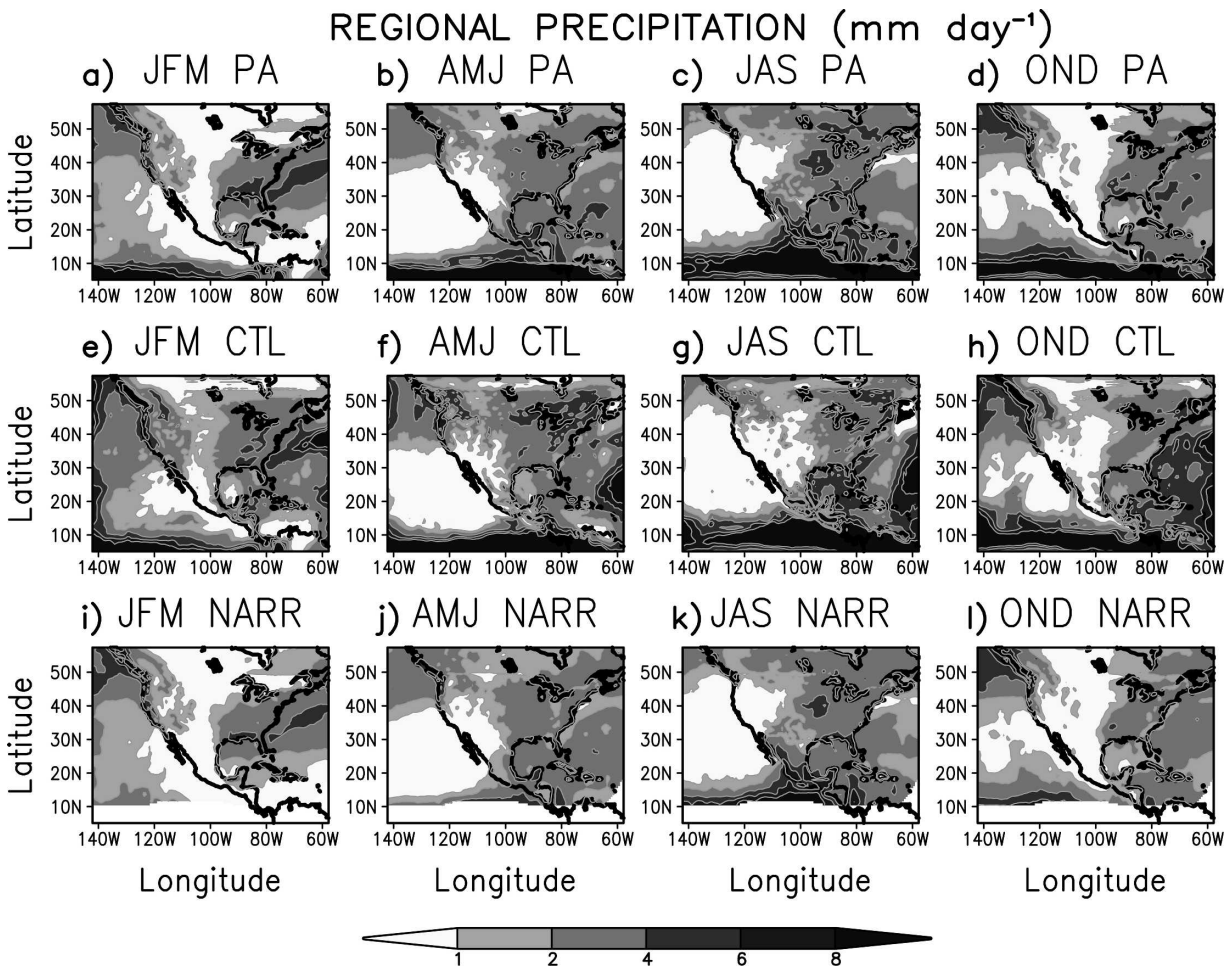

FIG. 1. Regional seasonal precipitation (mm day^{-1}) of the average of 1988 and 1993 over the entire experiment domain for (a)–(d) PA, (e)–(h) Control (CTL), and (i)–(l) NARR for winter (JFM), spring (AMJ), summer (JAS), and fall (OND).

NARR domain does not reach below 10°N as shown by the undefined values in Figs. 1i–k. The linear correlation coefficients and root-mean-square errors (RMSEs) between PA and NARR are, respectively, 0.98 (0.28 mm day^{-1}), 0.99 (0.29 mm day^{-1}), 0.99 (0.43 mm day^{-1}), and 0.99 (0.27 mm day^{-1}) for winter, spring, summer, and fall for the inner domain between 20° and 52°N and 130° and 70°W. For Control, the linear correlation coefficients and RMSEs are, respectively, 0.77 (1.24 mm day^{-1}), 0.73 (1.28 mm day^{-1}), 0.62 (1.49 mm day^{-1}), and 0.81 (1.19 mm day^{-1}) for the same inner domain. Including the sponge zone decreases the correlation and increases the RMSE of Control, as can be seen from the Control western/eastern noisy boundaries in Figs. 1e–h. The summer monsoon precipitation over Mexico and the southwestern United States is well represented in Figs. 1c,k by PA and NARR, and missed in Fig. 1g by Control. The dry season in Mexico, the central United States, and Canada during winter and fall is also well simulated by PA (Figs. 1a,d) and NARR (Figs. 1i,l), and not well represented by Control (Figs. 1e,h). The subtropical high is better defined in the PA and NARR precipitation fields in spring and summer (Figs. 1b,c and Figs. 1j,k) than in Control (Figs. 1f,g). It is evident from Fig. 1 that the PA scheme is able to reproduce the NARR precipitation input quite well during the four seasons.

a. Changes in the moisture fields

1) MOISTURE BUDGET

Floods over the upper Mississippi River basin characterized the summer of 1993 and a drought over the central part of United States marked the summer of 1988. It was because of this contrast that we chose 1988 and 1993 for the PA 1-yr simulations. Figure 2 compares the difference between the moisture budget terms of the 1993 and 1988 summers (June, July) from the

Unauthenticated | Downloaded 04/29/25 09:21 AM UTC

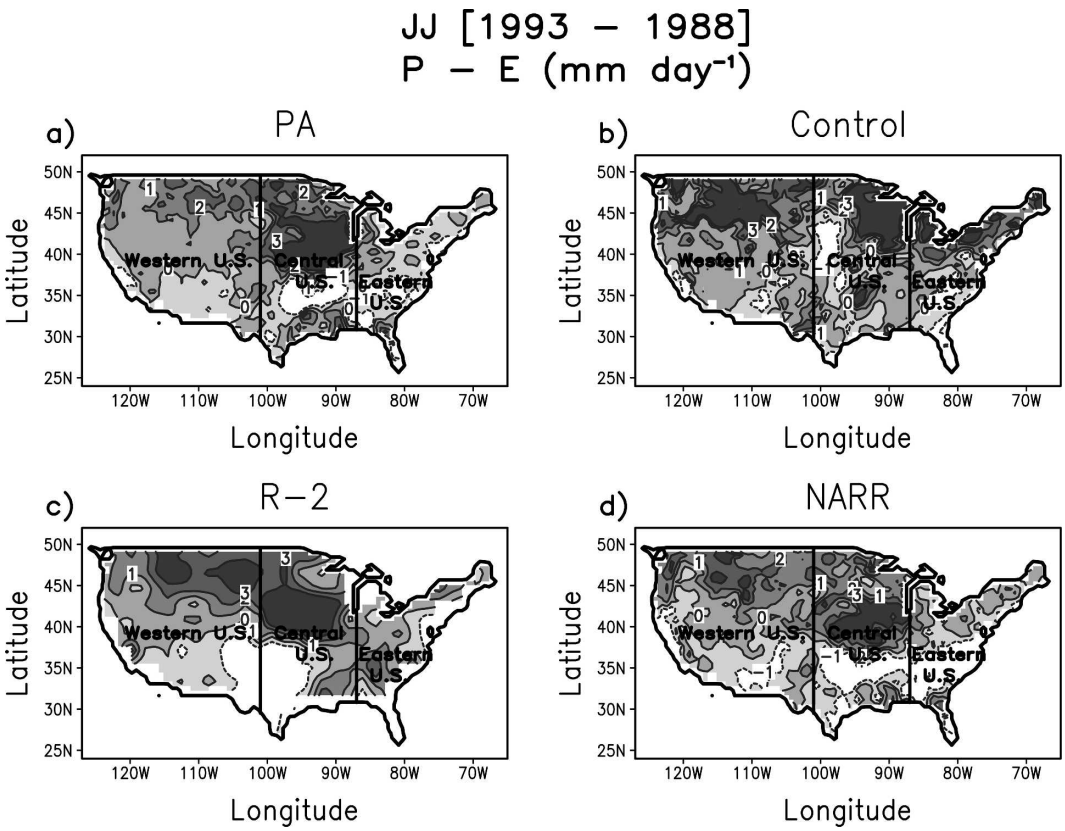

FIG. 2. June and July (1993–88) precipitation minus evaporation ($P - E$, mm day^{-1}) for (a) PA, (b) Control, (c) R-2, and (d) NARR over the three analyzed regions over CONUS.

difference between precipitation and evaporation (moisture convergence) for the analyzed U.S. subregions, namely, the western, central, and eastern regions. PA (Fig. 2a) and NARR (Fig. 2d) had remarkable similarities especially over central United States, while Control (Fig. 2b) was unsuccessful in representing the flood area in central United States as PA and NARR. Figure 2c shows a larger flood area for R-2 as well as a larger surface moisture flux to the atmosphere east of the southern Rocky Mountains.

2) SPECIFIC HUMIDITY VERTICAL PROFILES

Specific humidity is the PA scheme adjustment variable. Figures 3 and 4 display vertical profiles of the specific humidity differences of PA, Control, and R-2 with respect to NARR. Western, central, and eastern U.S. regions are represented in Figs. 3a–c and 4a–c because of the distinct precipitation regimes. The conterminous United States (CONUS) is also represented in Figs. 3d and 4d. Figures 3a and 4a show that the PA specific humidity vertical profile during the dry summer (1988) over the western United States noticeable differs from Control in the lower troposphere in comparison to the summer of 1993. This may be due to reduction of precipitation in the control simulation for the summer of 1988.

As mentioned previously in section 2, the PA scheme uses an arbitrary vertical layer when the model does not predict rain. These arbitrary layer limits were probably used more often during the 1988 summer than the 1993 summer, which explains why PA had specific humidity values greater than NARR in the middle troposphere only during the dry summer (Figs. 3a–d). Figure 4 shows the profile for the wet summer of 1993, which indicates that PA was closer to NARR than Control, especially over the central and eastern United States (Figs. 4b,c). R-2 is actually closer to NARR, but both reanalyses use a 3DVAR system, which directly affects prognostic variables.

b. PA impact on the surface water budget terms

In this section, we analyze the impact of long-term precipitation assimilation on the surface water budget. Figure 5 shows the average of the 1988 and 1993 regional mean seasonal cycle for precipitation, evaporation, runoff, and surface water corresponding to the

Unauthenticated | Downloaded 04/29/25 09:21 AM UTC

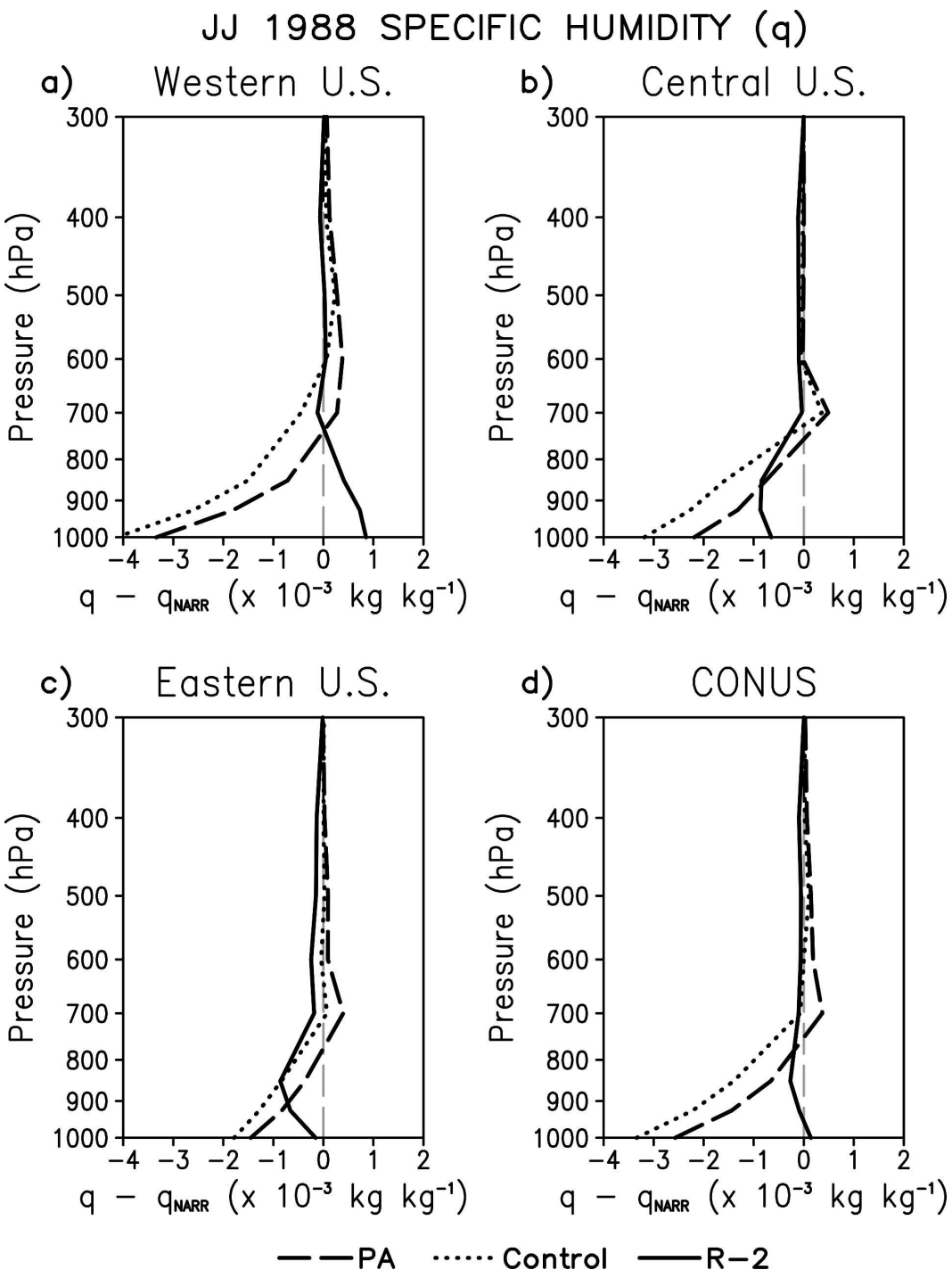

FIG. 3. June and July 1988 vertical profile of the specific humidity difference from NARR ($\times 10^{-3}$ kg kg^{-1}) over (a) western, (b) central, (c) and eastern United States, and (d) CONUS.

vertically integrated soil moisture plus water equivalent accumulated snow depth. PA shows a good agreement with NARR and Higgins's data [observed precipitation (OBS)] as shown by the dashed lines in Figs. 5a–c. On the other hand, Control has larger errors in both directions (under- and overestimation of precipitation, hereafter, dry and wet biases, respectively) as well as misplacement of the precipitation maxima. R-2 presents a systematic wet bias especially over the eastern United States during summer (Fig. 5c).

Unauthenticated | Downloaded 04/29/25 09:21 AM UTC

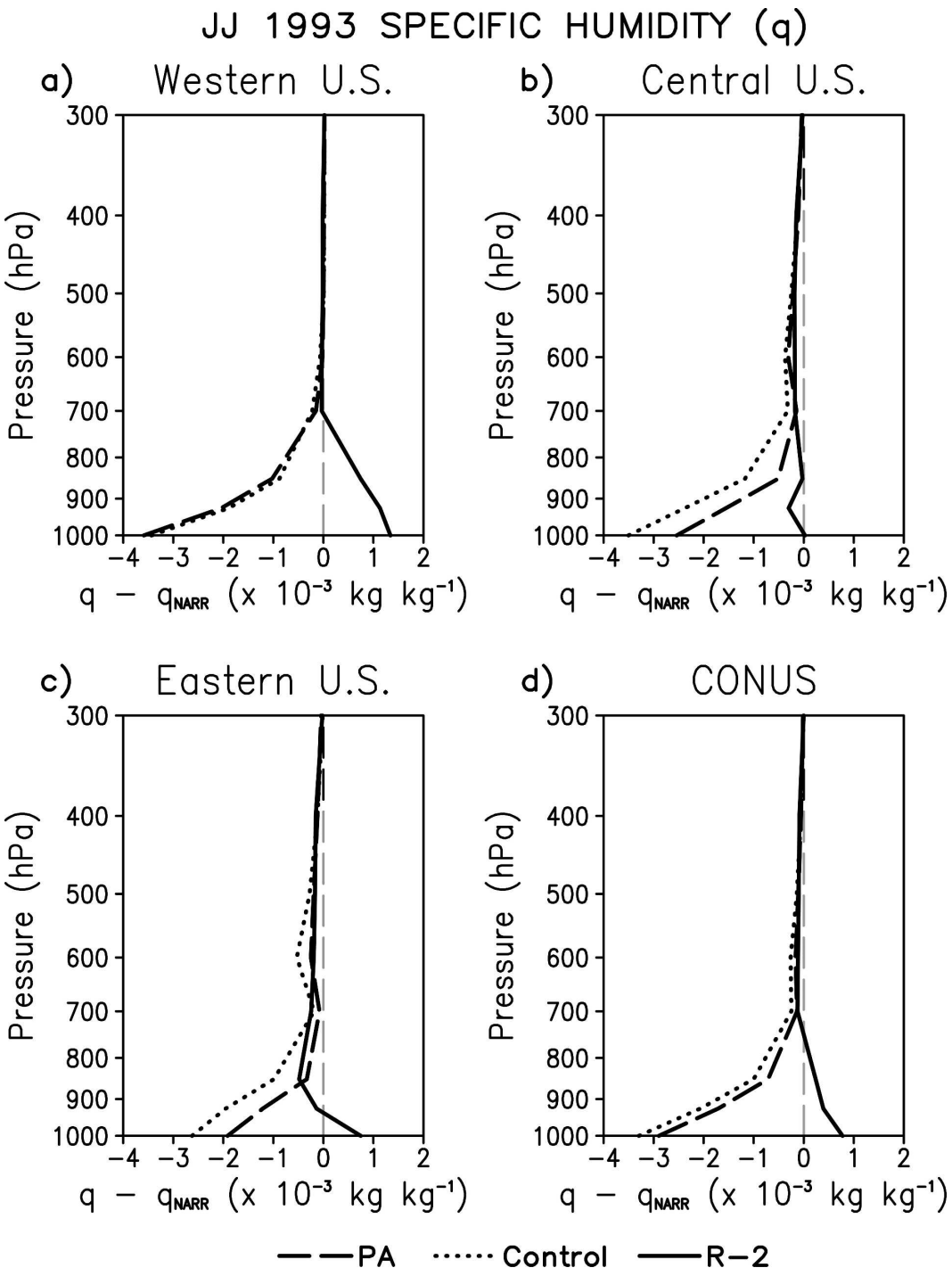

FIG. 4. June and July 1993 vertical profile of the specific humidity difference from NARR ($\times 10^{-3}$ kg kg^{-1}) over (a) western, (b) central, (c) and eastern United States, and (d) CONUS.

The analysis of the surface evaporation (Figs. 5d–f) shows similarities between PA and Control for the regional seasonal cycle. Overall, R-2 is similar to NARR, but overestimates the evaporation values. The evaporation monthly means reveal significant seasonality with a maximum around the warmer months. Control places the evaporation maximum over western and central regions in late spring rather than summer. PA and Control evaporation values are lesser than NARR and R-2 values over the eastern United States during sum-

Unauthenticated | Downloaded 04/29/25 09:21 AM UTC

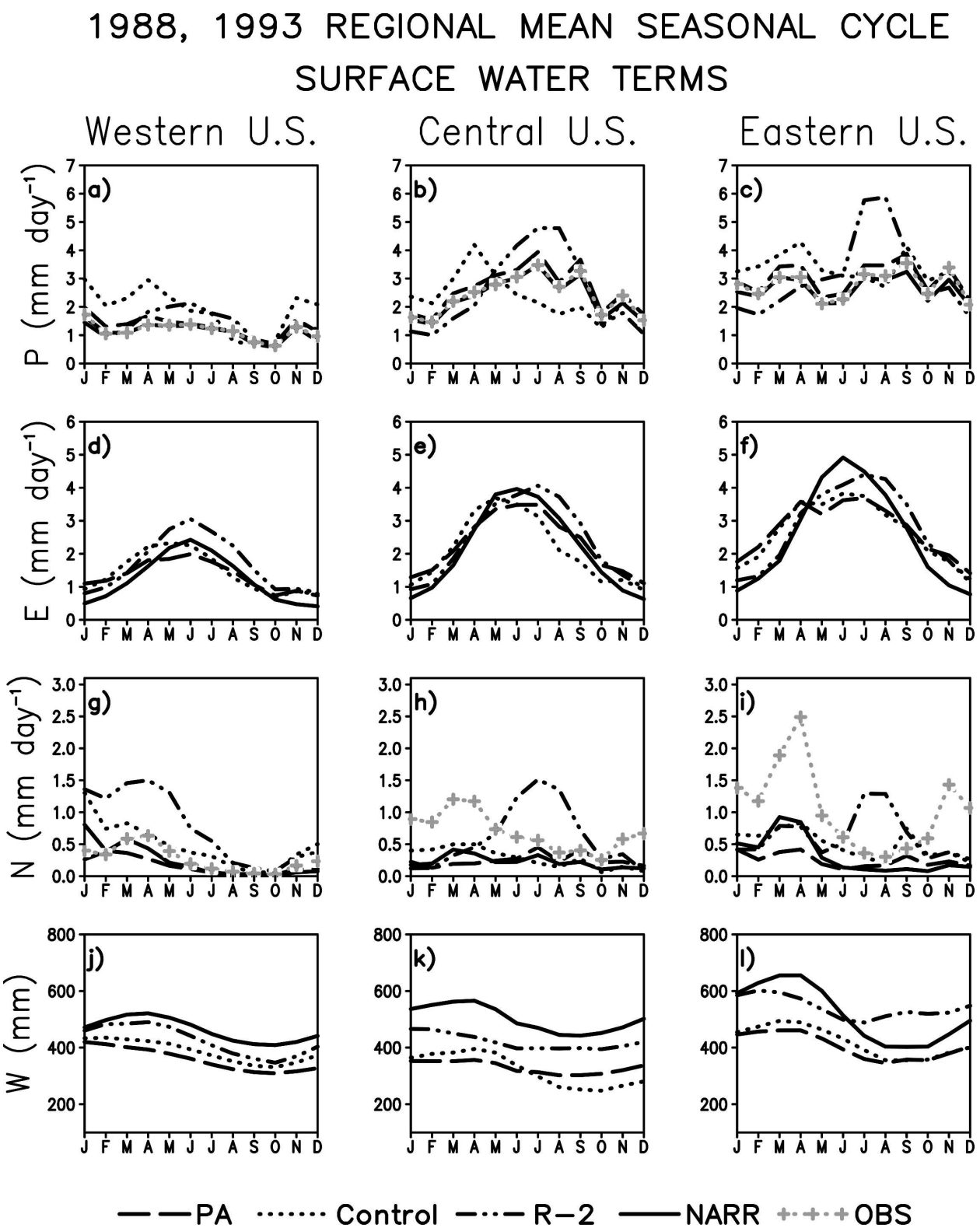

FIG. 5. Regional seasonal cycle of the average of 1988 and 1993 for (a)–(c) precipitation (P, mm day^{-1}); (d)–(f) evaporation (E, mm day^{-1}); (g)–(i) runoff (N, mm day^{-1}); and (j)–(l) surface water (W, mm) over western, central, and eastern United States.

Unauthenticated | Downloaded 04/29/25 09:21 AM UTC

mer. The evaporation over the central United States (Fig. 5e) is comparable but somewhat higher than the Maurer et al. (2001) evaporation for a 10-yr integration.

The UNH runoff (observed runoff or OBS) has the largest runoff monthly means during spring and fall over eastern United States, whereas R-2 had the largest runoff monthly mean over central and eastern United States during summer (Figs. 5h–i). PA had the lowest runoff values followed by NARR and Control. The low PA runoff values result from a diminution of precipitation, which in general is overestimated in Control, and the impact of the land surface model (OSU2). Runoff generation needs to be further improved in these land surface models.

Although surface water comparisons cannot easily be made between different land surface schemes, a brief discussion of the surface water regional annual cycles is introduced through Figs. 5j–l. Surface water (W) combines the vertically integrated soil moisture with the total of the subsurface layers corresponding here to a thickness of 2 m for all models, and water equivalent accumulated snow depth. The Noah land surface scheme used by NARR had the highest surface water values over all regions, except for the eastern United States in the second half of the year. R-2 utilized a version of the OSU land surface model (OSU1), and provided the second highest surface water value over the continental United States. The slow changes in the surface water behavior throughout the year indicate that the surface water annual cycle is small, as seen in Figs. 5j–l. Surface water has a maximum around March–April, and a minimum around September–October for the regional simulations and reanalysis over all three regions. R-2 and PA had almost no annual variation over the central domain. The differences in the R-2 annual cycle may be related to the precipitation forcing applied to the soil moisture prognostic equation. Control and PA use the same land surface model, and therefore have comparable surface water values.

Figure 6 is similar to Fig. 5 except that it shows the difference between 1993 and 1988 regional seasonal cycles. The climatology influence was removed by making this difference. Basically, Fig. 6 shows the interannual differences. Note that PA precipitation difference agrees quite well over the entire United States with NARR and OBS (Figs. 6a–c). Control and R-2 differ from PA, NARR, and OBS mostly over the eastern domain.

Evaporation differences (Figs. 6d–f) are remarkable over the central United States during summer for NARR and Control, and spring–summer for R-2 and PA. Figures 6b,e suggest that about half of the precipitation differences resulted from evaporation.

Figures 6g–i show that runoff differences for PA, Control, and NARR have more contrast with OBS differences over the central United States; R-2 has runoff difference maxima over the western and central United States, and NARR has the maximum runoff differences during spring over the eastern United States, similar to the OBS.

Surface water differences (Figs. 6j–l) are smaller over the western United States, and larger during the summer over the central United States and spring–summer over the eastern United States, with reduction of differences in May over the eastern United States for all simulations, which agrees with Fig. 6c for precipitation.

Figures 7a,b show the linear correlation coefficients for 1988, 1993 precipitation and runoff averages, and differences over CONUS. PA, Control, NARR, and R-2 are compared to Higgins's precipitation and the UNH/EOS runoff datasets. The PA and NARR precipitation features correlate above 0.9 with the observations. There is not a significant improvement for PA runoff from Control, respectively, above 0.5 and 0.4. However, PA runoff difference was considerable increased from Control (Fig. 7b). Both correlation coefficients (Figs. 7a,b) indicate that PA increases precipitation and runoff correlations from Control and R-2.

The surface water mass conservation equation (Roads et al. 2003) is given by

$$\frac{\partial W}{\partial t} = P - E - N + \text{Res}, \tag{2}$$

where P, E, and N are, respectively, precipitation, evaporation, and runoff, and Res corresponds to an artificial residual forcing or nonclosure term, which is not part of the physical solution but a term added to the prognostic equations by an external forcing. Figure 8 displays the 1988 and 1993 average regional surface water budget nonclosure term seasonal cycles for PA, Control, R-2, and NARR. Because they are continuous simulations, PA and Control are very close to zero; closure terms for the PA and Control were different than zero only because of various interpolation errors. By contrast, the NARR nonclosure term had excess values during winter, presumably due in part to the daily update of the NARR snow water equivalent from the daily global snow depth analysis of the U.S. Air Force (Mesinger et al. 2006). R-2 also had higher nonclosure term, especially over the western United States (Fig. 8a), mainly because the land surface model was substantially corrected by a soil moisture adjustment based on the difference between observed and model precipitation (Lu et al. 2005).

Unauthenticated | Downloaded 04/29/25 09:21 AM UTC

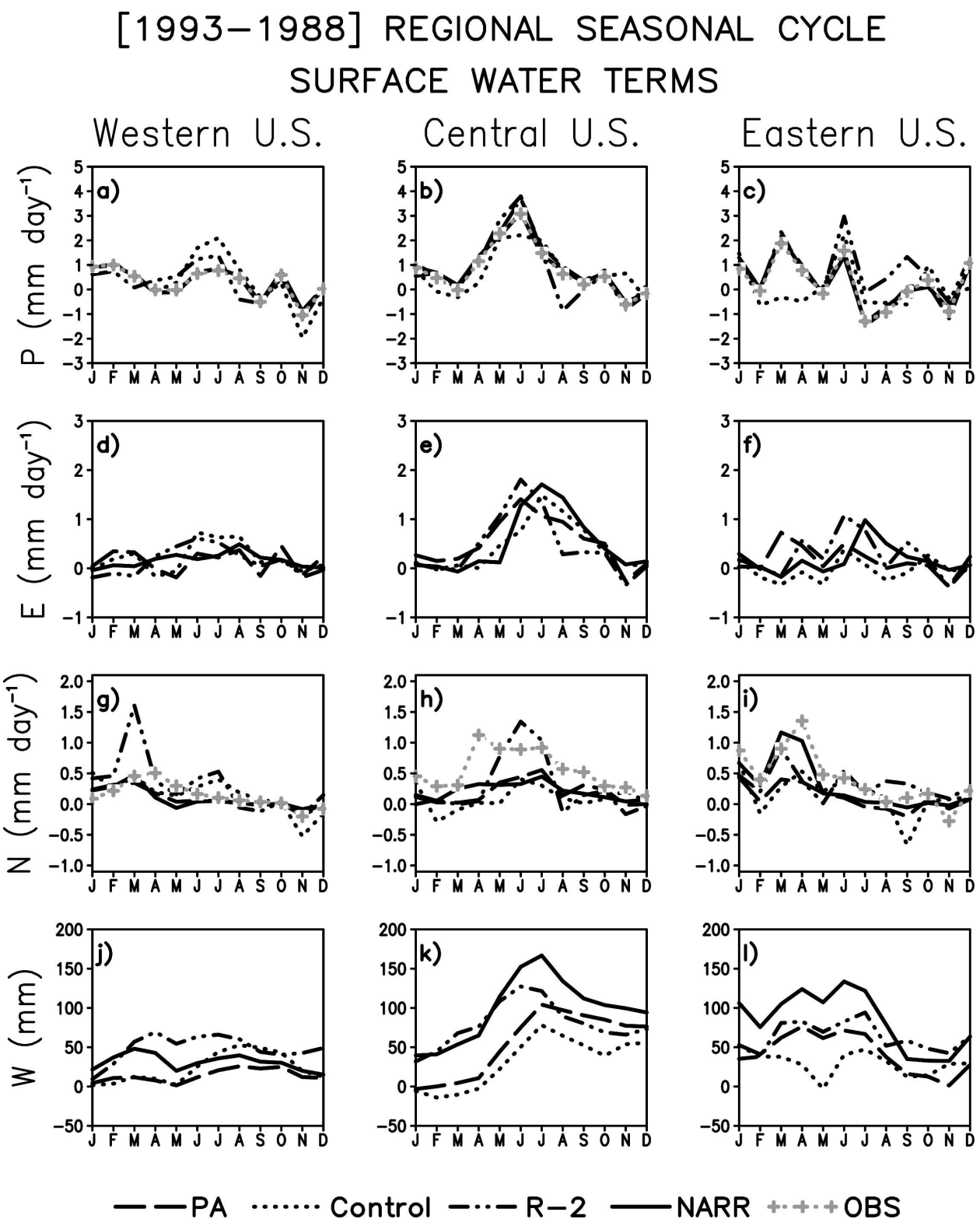

FIG. 6. Regional seasonal cycle of the difference between 1993 and 1988 for (a)–(c) precipitation *(P*, mm day^{-1}); (d)–(f) evaporation (*E*, mm day^{-1}); (g)–(i) runoff (*N*, mm day^{-1}); and (j)–(l) surface water (*W*, mm) over western, central, and eastern United States.

Unauthenticated | Downloaded 04/29/25 09:21 AM UTC

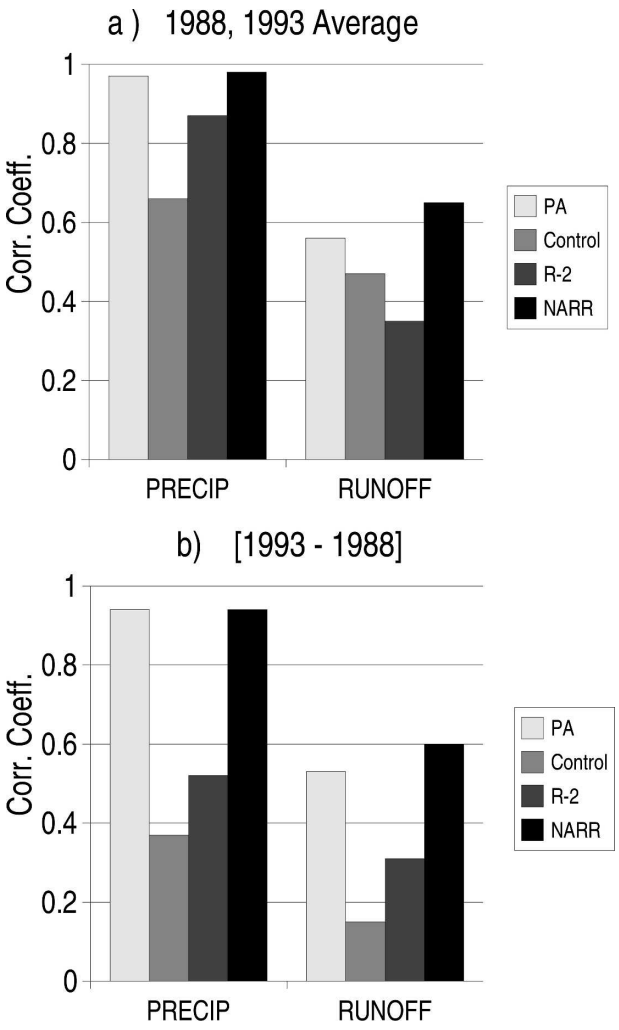

FIG. 7. Precipitation and runoff linear correlation coefficients for PA, Control, R-2, and NARR obtained over CONUS for (a) the 1988 and 1993 average and (b) the difference between 1993 and 1988. Higgins's data and UNH/EOS provided the observed values for precipitation and runoff, respectively.

c. PA impact on the surface energy budget terms

Betts et al. (1996) pointed out that many climate features rely on the land surface–atmosphere physical process interactions. In this context, a numerical model's surface energy budget can help us to understand the land surface–atmosphere system gain–loss of energy (Berbery et al. 1999).

The net radiation flux at the surface, Q_{rad}, consisting of solar radiation, SW, and terrestrial radiation, LW, is the driving force for the surface energy budget. The surface energy budget can be written in simplified form as

$$-Q_{\text{rad}} = Q_{\text{sen}} + Q_{\text{lat}} - Q_g, \tag{3}$$

where the upward fluxes are positive. Here Q_{sen} is the sensible heat flux, Q_{lat} is the latent heat flux, and Q_g is the ground heat flux. Neglecting the contribution of heat release due to snowmelt, then $Q_{\text{sfc}} \equiv Q_{\text{sen}} + Q_{\text{lat}} - Q_g$ is the total surface heat flux or response term to the external forcing Q_{rad} for a zero thickness layer, where there is no mass involved, and, consequently, no intake of internal energy (Stull 1988). For long-term integrations (annual means), we can easily assume very small Q_g values; that is, the surface net radiation flux will be balanced by the surface sensible and latent heat fluxes.

The soil moisture drives the partitioning of sensible and latent heat fluxes for the surface energy balance. The Bowen ratio (BR), which is the ratio of sensible and latent heat fluxes, characterizes the contribution of each of these terms, and will also be discussed later in this section.

In this section, the SRB surface radiation fluxes were used to evaluate simulations for 1988 and 1993. Tables 1a,b summarize the surface radiation budget terms over the western, central, and eastern United States for PA, Control, R-2, NARR, and SRB for 1988 and 1993. The net radiation flux at the surface is divided into upward and downward LW radiation fluxes, and surface upward and downward SW radiation fluxes, respectively, Q_{ulw}, Q_{dlw}, Q_{usw}, and Q_{dsw}. The net surface radiation and total surface heat fluxes, Q_{rad} and Q_{sfc}, and BR are also displayed in Tables 1a,b.

The PA annual Q_{ulw} values for both years are comparable to Control and higher than SRB (Tables 1a,b), which leads us to conclude that the surface temperatures for PA and Control should also be higher than the observed. Figures 9a–c and 10a show that during summer Control surrounds the SRB Q_{ulw} values. PA balances the annual Q_{ulw} with positive mean bias error (MBE) during winter and negative MBE during summer (Fig. 10a). NARR also has higher Q_{ulw} annual values over the western United States (Tables 1a,b), indicating reduction of precipitation over that region. The higher NARR Q_{ulw} values can also be found in Figs. 9a and 10a, which show positive NARR Q_{ulw} MBE during the whole year. R-2 is closer to the SRB Q_{ulw} annual values (Tables 1a,b), with an increased difference for Q_{ulw} over the central United States for both years. R-2, as PA, also balances the Q_{ulw} annual average over CONUS with positive MBE during winter and negative MBE during most of summer (Fig. 10a).

PA surface downward LW flux has the second highest values among the simulations for all regions (Tables 1a,b). The PA Q_{dlw} values are also closer to the SRB values than Control and R-2. Higher Q_{dlw} suggests an increase of the cloud cover, and also explains the lowest western Q_{dlw} values for PA, Control, R-2, and NARR. Figures 9d–f and 10b show that SRB has higher Q_{dlw} values, and that PA and NARR Q_{dlw} seasonal cycles

Unauthenticated | Downloaded 04/29/25 09:21 AM UTC

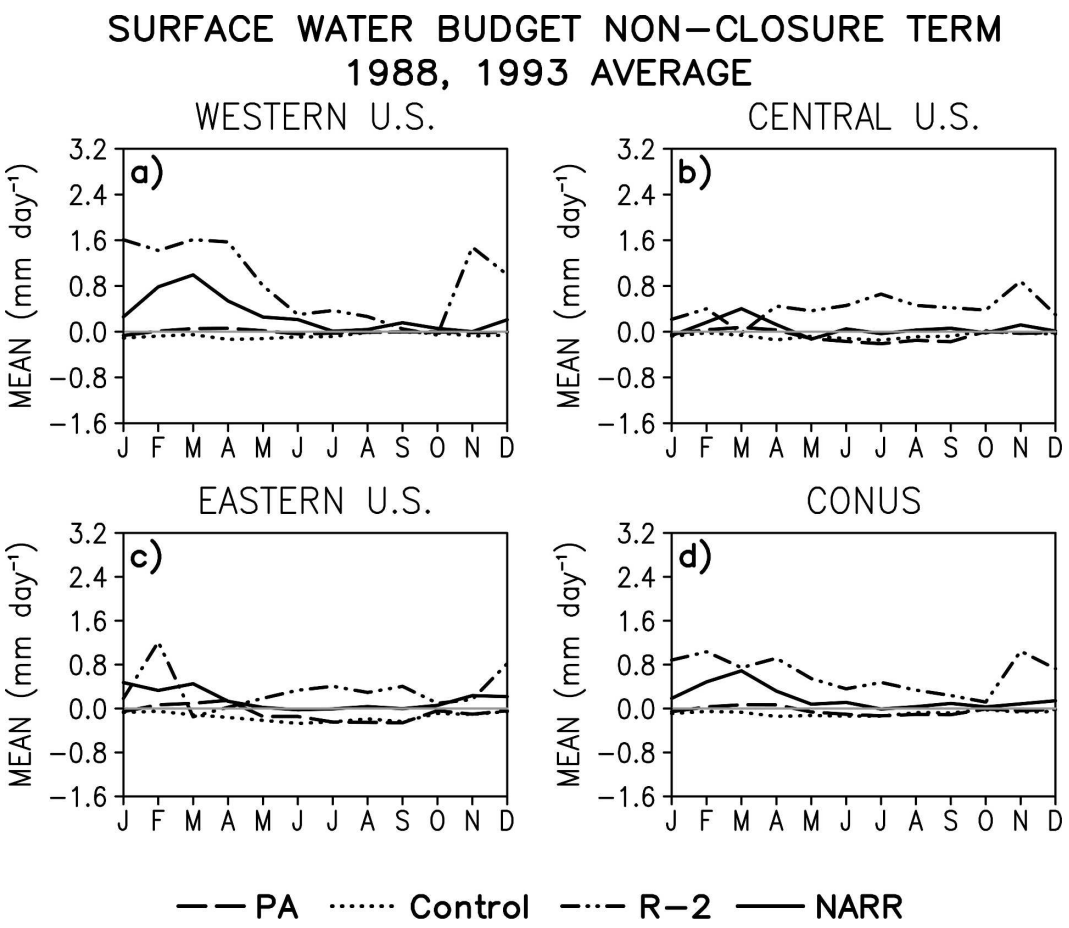

FIG. 8. Surface water budget nonclosure term (mm day^{-1}) for the 1988 and 1993 average over (a) western, (b) central, (c) and eastern United States, and (d) CONUS.

TABLE 1a. Surface energy budget term annual means for western, central, and eastern United States for 1988.

Region	1988	PA	Control	R-2	NARR	SRB
Western	Q_{ulw}	367	368	361	379	363
Western	Q_{dlw}	273	271	266	275	289
Western	Q_{usw}	39	43	53	63	26
Western	Q_{dsw}	212	216	224	239	176
Western	Q_{rad}	−79	−76	−76	−72	−76
Western	Q_{sfc}	80	77	68	79	
Western	BR	1.33	1.17	0.69	1.84	
Central	Q_{ulw}	391	393	384	393	375
Central	Q_{dlw}	316	311	303	317	318
Central	Q_{usw}	29	34	41	59	22
Central	Q_{dsw}	191	200	215	226	174
Central	Q_{rad}	−87	−84	−93	−91	−95
Central	Q_{sfc}	85	82	89	102	
Central	BR	0.52	0.58	0.43	1.07	
Eastern	Q_{ulw}	383	382	373	382	371
Eastern	Q_{dlw}	317	310	301	320	321
Eastern	Q_{usw}	24	27	38	52	18
Eastern	Q_{dsw}	181	192	207	208	161
Eastern	Q_{rad}	−91	−92	−97	−94	−93
Eastern	Q_{sfc}	88	89	93	104	
Eastern	BR	0.16	0.15	0.18	0.46	

TABLE 1b. Surface energy budget term annual means for western, central, and eastern United States for 1993.

Region	1993	PA	Control	R-2	NARR	SRB
Western	Q_{ulw}	361	361	355	373	353
Western	Q_{dlw}	272	270	268	276	283
Western	Q_{usw}	38	41	54	63	27
Western	Q_{dsw}	208	211	220	234	175
Western	Q_{rad}	−81	−79	−79	−74	−78
Western	Q_{sfc}	80	79	68	82	
Western	BR	1.10	0.90	0.56	1.50	
Central	Q_{ulw}	388	390	376	384	369
Central	Q_{dlw}	320	316	307	321	318
Central	Q_{usw}	27	32	43	56	26
Central	Q_{dsw}	184	192	205	212	160
Central	Q_{rad}	−89	−86	−93	−93	−83
Central	Q_{sfc}	90	86	90	102	
Central	BR	0.23	0.27	0.19	0.54	
Eastern	Q_{ulw}	383	384	372	382	372
Eastern	Q_{dlw}	322	316	307	326	324
Eastern	Q_{usw}	24	28	40	50	26
Eastern	Q_{dsw}	179	188	201	200	157
Eastern	Q_{rad}	−94	−92	−96	−94	−83
Eastern	Q_{sfc}	90	87	93	103	
Eastern	BR	0.10	0.15	0.07	0.35	

Unauthenticated | Downloaded 04/29/25 09:21 AM UTC

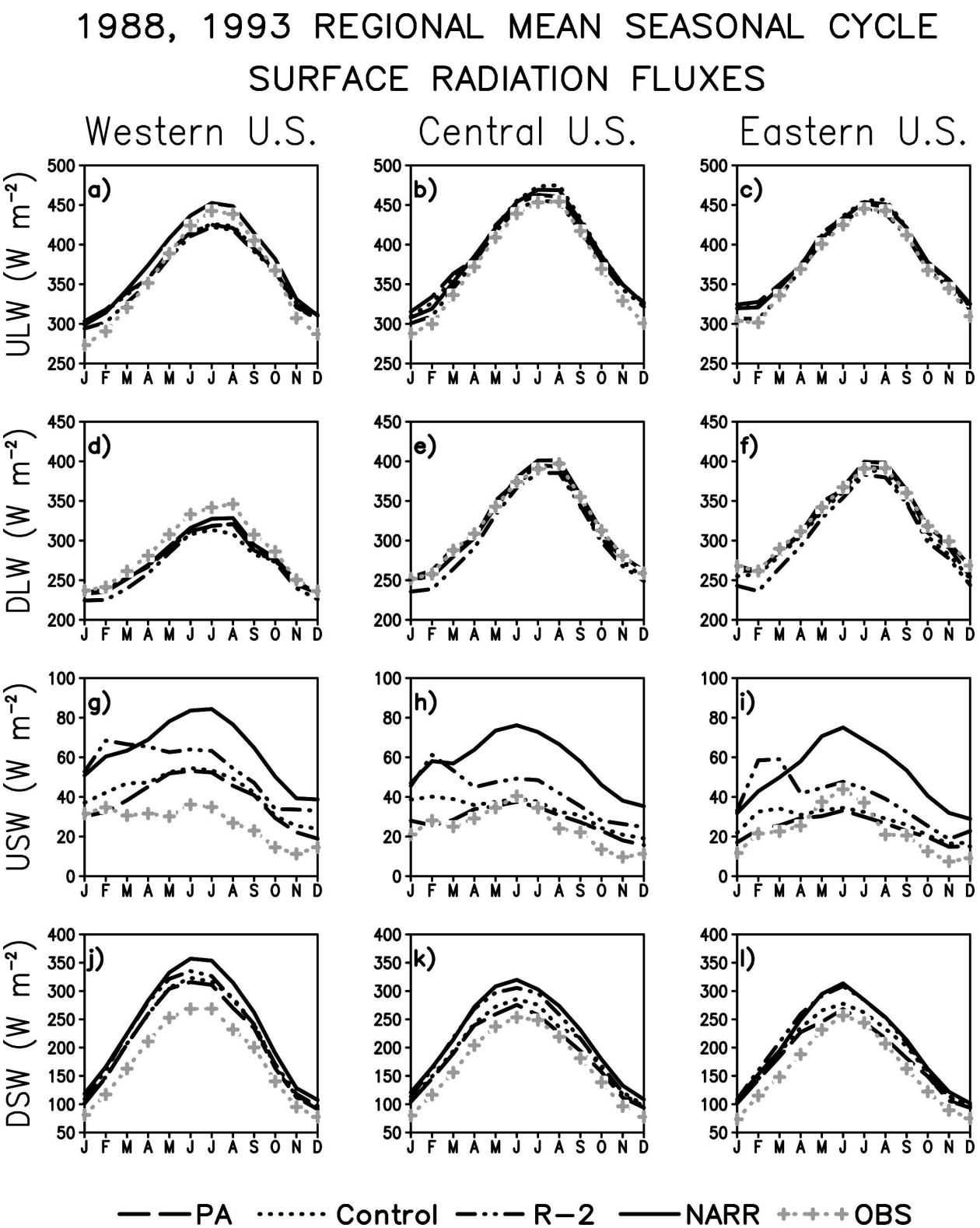

FIG. 9. The 1988 and 1993 regional mean seasonal cycle of the surface radiation fluxes (W m^{-2}) of (a)–(c) upward LW (ULW); (d)–(f) downward LW (DLW); (g)–(i) upward SW (USW); and (j)–(l) downward SW (DSW) over western, central, and eastern United States.

Unauthenticated | Downloaded 04/29/25 09:21 AM UTC

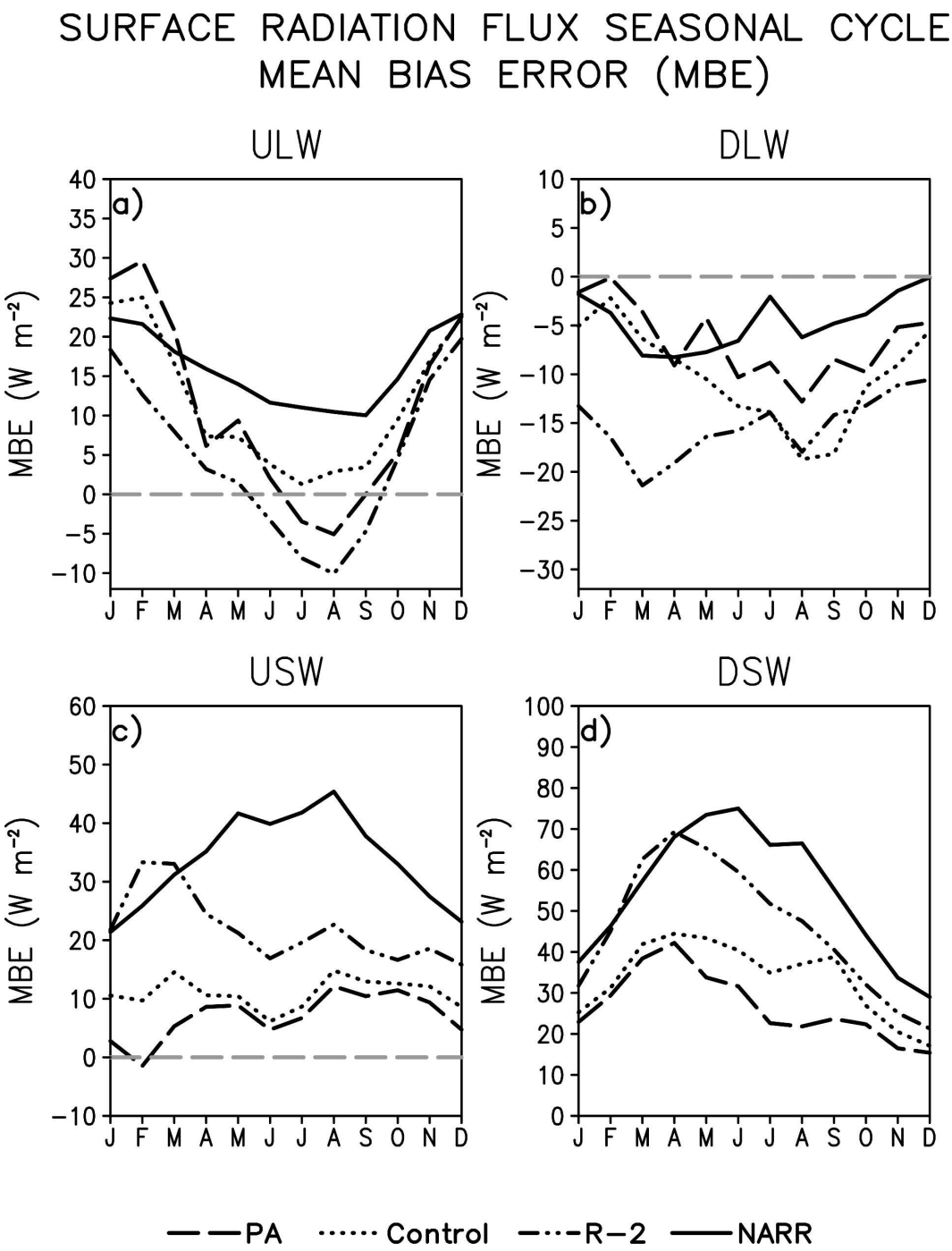

FIG. 10. Seasonal cycle of the mean bias error (MBE) of the (a) upward LW (ULW), (b) downward LW (DLW), (c) upward SW (USW), and (d) downward SW (DSW) radiation fluxes (W m^{-2}) over CONUS for the average of 1988 and 1993.

are also closer to the SRB annual cycle, with lower absolute MBE values for NARR over CONUS during summer and winter. R-2 has the highest Q_{dlw} absolute MBE values especially in spring (Fig. 10b), and the lowest annual Q_{dlw} values for both years in all regions (Tables 1a,b). Because there was almost a balance between Q_{ulw} and Q_{dlw}, the main contribution to Q_{rad} comes from the surface SW radiation fluxes.

The upward SW radiation flux is the smallest component of the net radiation flux at the surface, and

Unauthenticated | Downloaded 04/29/25 09:21 AM UTC

depends on the model's choice of surface albedo. In direct contrast with the PA surface LW radiation fluxes, PA surface SW radiation fluxes have the lowest mean values (Figs. 9g–i and Tables 1a,b), approaching the SRB Q_{usw} values. Figures 9g–i also show winter–spring Q_{usw} maximum for R-2 particularly over the eastern United States, which may be related to the R-2 surface characteristics and the presence of snow. As shown in Fig. 10c, PA Q_{usw} has the lowest MBE over CONUS for all months. NARR has the highest Q_{usw} values (Tables 1a,b), and the highest upward SW radiation flux MBEs over CONUS almost the entire year (Fig. 10c). This increased NARR Q_{usw} is particularly noticeable in summer, as shown in Fig. 10c. Control Q_{usw} follows PA closely, except for late winter and early spring, where PA Q_{usw} has its best performance. R-2 Q_{usw} values stay between Control and NARR curves.

The dominant component of the net SW radiation flux at the surface is Q_{dsw}, which can be several times higher than the annual mean of Q_{usw}. The surface downward SW radiation flux is inversely related to the cloud cover, which explains the reduced PA annual surface downward SW radiation flux, especially over the eastern United States The Q_{dsw} regional mean seasonal cycle and the annual values are shown in Figs. 9j–l and Tables 1a,b, with lowest values for SRB followed by PA, and highest values for NARR. Table 1b shows that, over the eastern United States, Q_{dsw} has also reduced annual values for 1993 for PA, Control, R-2, and NARR. In general the annual surface radiation fluxes had lower values in 1993 than 1988. PA Q_{dsw} MBE is the smallest over CONUS during the whole year followed by Control (Fig. 10d). NARR and R-2 have higher Q_{dsw} annual values for all three regions (Tables 1a,b), and the higher MBE values for the entire year over CONUS (Fig. 10d).

Figures 11a–l show the difference between 1993 and 1988 for the regional surface radiation fluxes. Overall the simulations followed the SRB difference curves, showing increased surface radiation flux values in 1988 especially during late spring and early summer. The main differences with respect to the SRB values were found for the surface upward SW fluxes, indicating increased Q_{usw} for 1993 (Figs. 11h–i). In the late spring of 1993 over the central United States (Fig. 11k) Q_{dsw} is markedly reduced because the augmentation of condensed water due to the increase of precipitation, noticeable for NARR, is in agreement with the observations (SRB).

As shown in Eq. (3), the external forcing is balanced by the total surface heat flux, and we can expect that Q_{rad} should be close to Q_{sfc}. However, the atmospheric radiation fluxes are not usually integrated at each model's time step, mainly because the atmospheric numerical model's radiation schemes have an expensive computational cost. Pauluis and Emanuel (2004) discussed how this infrequent calculation of the radiation fluxes can lead to an unbalanced model surface energy budget, which could explain the differences reported in Tables 1a,b. The balance assumption works for PA, Control, and R-2; by contrast NARR tends to have higher values for Q_{sfc}, which are apparently greater than the NARR surface net radiation flux (Tables 1a,b). The NARR difference between Q_{rad} and Q_{sfc} may be due to an increased NARR Q_{sen}, as shown in Figs. 12a–c, whereas NARR surface latent heat fluxes are comparable to the other simulations (Figs. 12d–f). Differences between the surface temperature and the 2-m air temperature for the 1988 and 1993 average are shown in Fig. 13. The shaded areas represent differences above 1° (dark gray) and below −1° (light gray). The NARR positive values over the CONUS are consistent with the higher NARR Q_{sen} values displayed in Figs. 12a–c. R-2 has the lowest Q_{sfc} values over the western United States, which is also consistent with Fig. 12a and the annual difference in Fig. 13c. PA and Control have similar features with higher upward sensible heat flux values over the central United States southeast of the Rocky Mountains.

Figures 12g–l show the Q_{sen} and Q_{lat} regional differences between 1993 and 1988. These differences are enhanced over the central United States because of dissimilarity in the precipitation features for these years (Figs. 12h,k), although the absolute maxima are not exactly in phase.

BR values are also displayed in Tables 1a,b, and point out the differences between the three regions and between dry and wet years. According to the Köppen Climate Classification, the western U.S. climate varies from a Mediterranean climate (on the California coast) to a dry tropical climate or desert (east of the Rocky Mountains). BR > 1 represents dry regions like the western United States, where the sensible heat flux gives the major contribution to the balance with the radiation term. The central and eastern United States have more latitudinal climate variations, with a predominant moist continental climate. The NARR, PA, and Control BR values characterize western United States as semiarid. R-2 BR has not shown any clear distinction between semiarid and moist continental climate characteristics, which might partially be related to the use of a lesser detailed vegetation by the land surface model. All simulations had a higher BR during the dry year over the central United States, which indicates a higher Q_{sen} contribution during 1988 over this region.

Unauthenticated | Downloaded 04/29/25 09:21 AM UTC

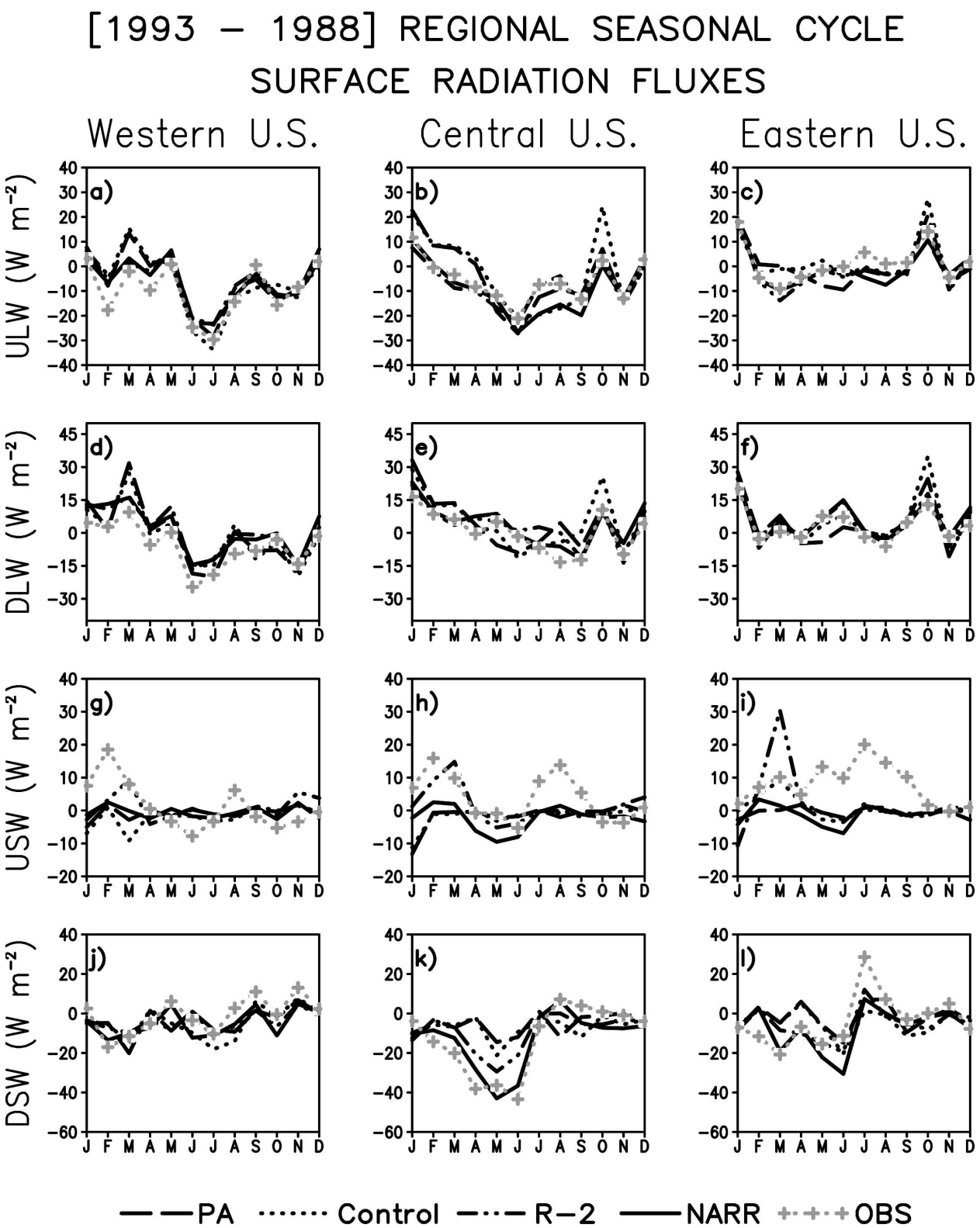

FIG. 11. The 1988–93 regional seasonal cycle of the surface radiation fluxes (W m^{-2}) of (a)–(c) upward LW (ULW); (d)–(f) downward LW (DLW); (g)–(i) upward SW (USW); and (j)–(l) downward SW (DSW) over western, central, and eastern United States.

Unauthenticated | Downloaded 04/29/25 09:21 AM UTC

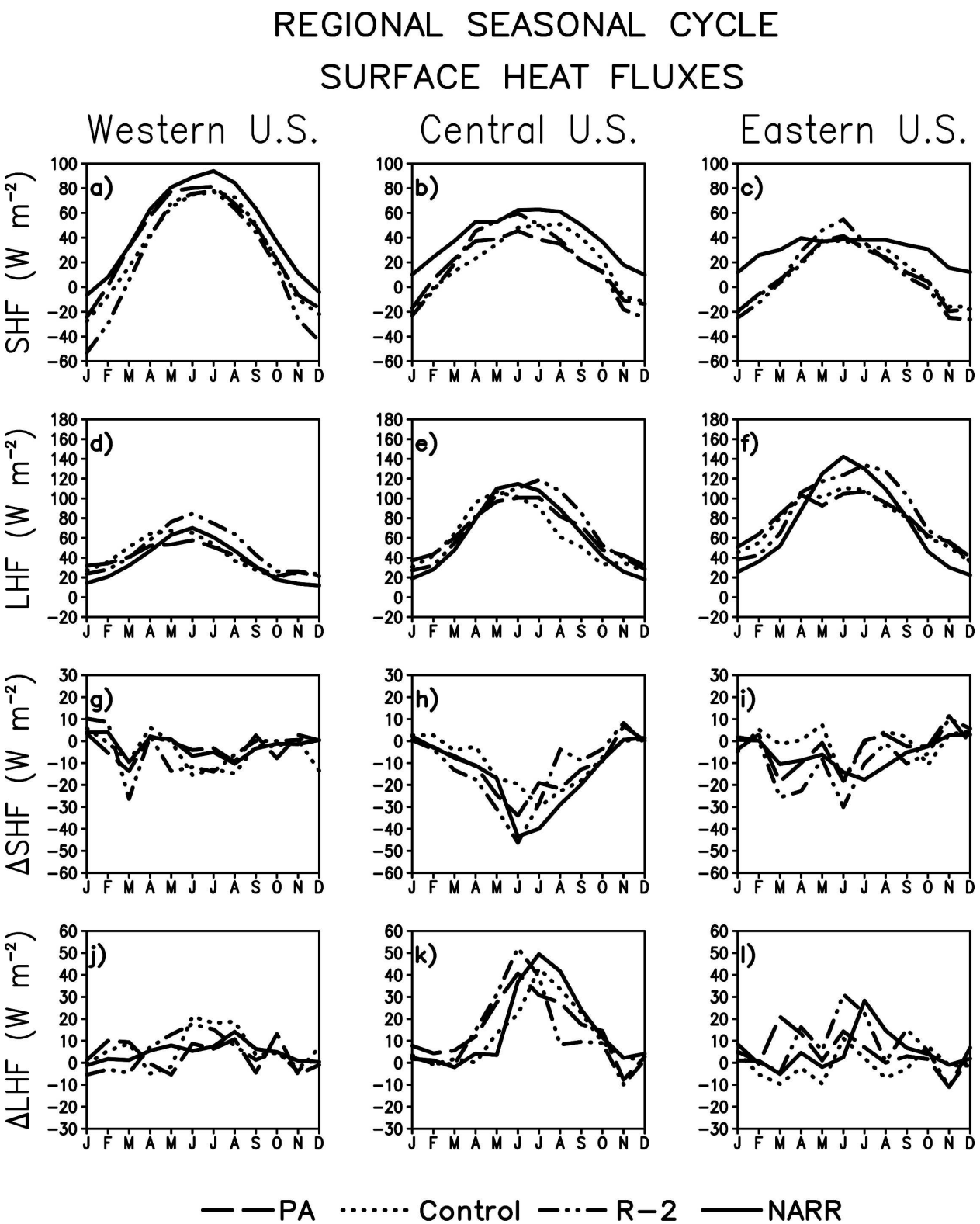

FIG. 12. Regional seasonal cycle of the surface heat fluxes (W m^{-2}) of (a)–(c) sensible heat flux (SHF) average; (d)–(f) latent heat flux (LHF) average; (g)–(i) SHF difference (ΔSHF); and (j)–(l) LHF difference (ΔLHF) over western, central, and eastern United States.

Unauthenticated | Downloaded 04/29/25 09:21 AM UTC

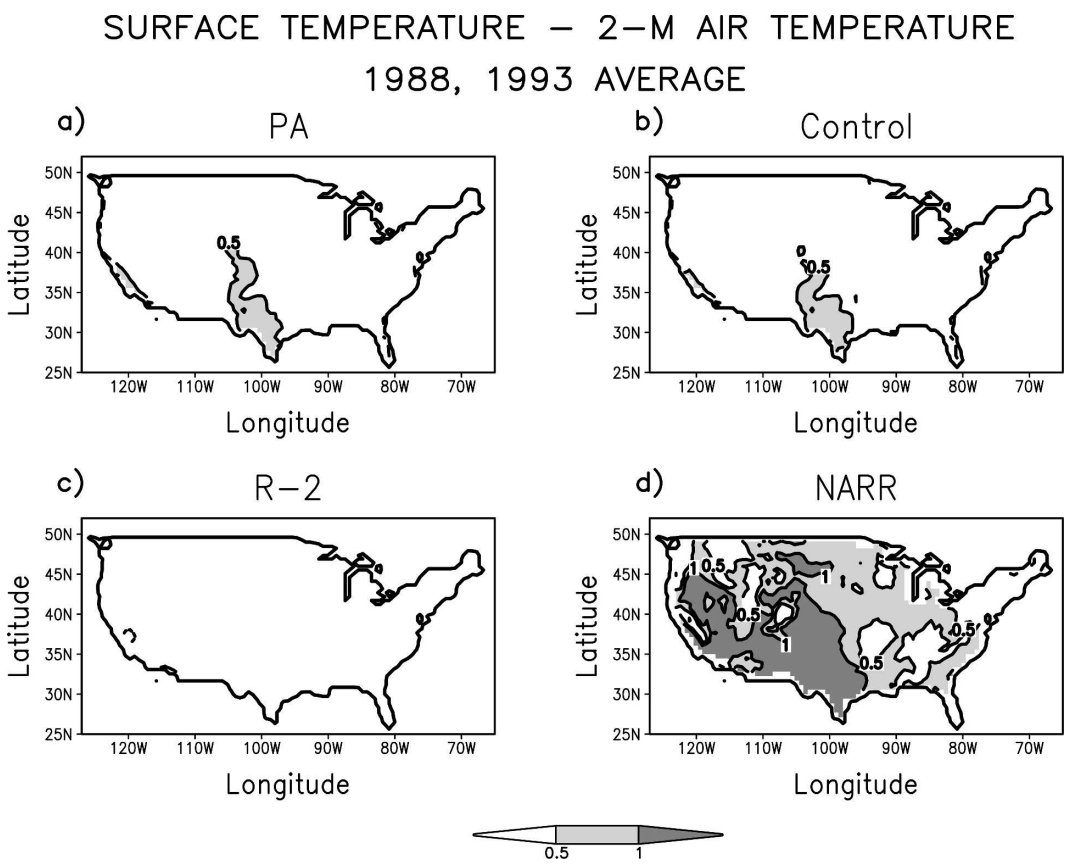

FIG. 13. Difference between surface temperature and 2-m air temperature for the 1988 and 1993 average of (a) PA, (b) Control, (c) R-2, and (d) NARR.

CRUTEM2 were used to evaluate the 2-m air temperature differences between 1993 and 1988 (Fig. 14). Basically PA and NARR have the lowest differences with respect to CRUTEM2. PA and Control had mostly higher differences than CRUTEM2 east of the Rocky Mountains and over the Mississippi River basin (Figs. 14a,b). However the higher PA difference values were confined to the western lower part of the basin, suggesting that precipitation assimilation was most effective over the upper Mississippi River basin during the 1993 floods. R-2 (Fig. 14c) shows a dipole with differences above 1° (dark gray area) to the east of the western United States, and below −1° (light gray area) mostly over the northern part of the central United States, which is similar to NARR over this area. Table 2 shows that the surface and 2-m air temperatures were usually higher in 1988 than 1993. NARR agreed well with CRUTEM2 (Fig. 14d and Table 2, here combined with the absolute temperatures for the base period 1961–90), and showed higher surface temperature values mostly over the western United States (Table 2), which would explain the increased NARR Q_{ulw} over the CONUS (Fig. 10a). By contrast, R-2 had the lowest 2-m air and surface temperature values. PA, Control, and R-2 usually had small differences between surface and 2-m air temperatures (Figs. 13a–c and Table 2), whereas the NARR 2-m air and surface temperature differences were higher (Fig. 13d and Table 2), which again is consistent with increased NARR surface sensible heat fluxes.

4. Concluding remarks

The precipitation assimilation methodology and analysis presented here was our first attempt to develop a long-term moisture-adjusted regional climate simulation. Although assimilation of precipitation was originally developed to increase short-term precipitation forecast skill, one of the additional advantages is that it can also provide better climatological surface water and energy fields. Thus precipitation assimilation could eventually improve coupled atmosphere–land interactions, which may ultimately prove to be useful for initializing long-range forecasts with greater forecast skill.

Unauthenticated | Downloaded 04/29/25 09:21 AM UTC

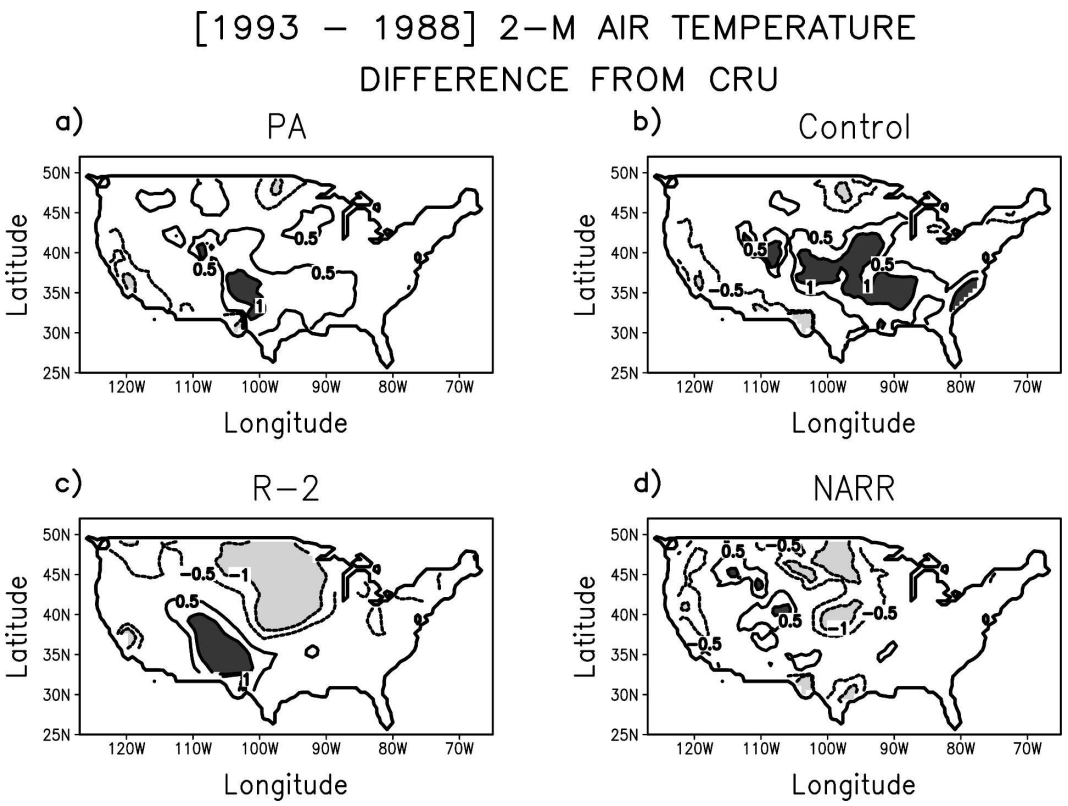

FIG. 14. The 1988–93 2-m air temperature difference with respect to CRU for (a) PA, (b) Control, (c) R-2, and (d) NARR. The light gray areas show differences below −1° and the dark gray areas display differences above 1°.

Vertical humidity profiles were adjusted by the PA scheme according to the differences between the 3-hourly NARR rain rates and the model's predicted rain rates in order to improve our regional model precipitation. Despite the simplicity of the PA approach used in this study, PA brought the ECPC-RSM precipitation fields closer to the NARR precipitation input, with a linear correlation coefficient closer to 1, and decreased RMSE. Another interesting aspect was the PA removal of the precipitation western/eastern boundary "noise" seen in Control. In this study, PA scheme was also more successful in adjusting the specific humidity vertical profiles with respect to NARR during the wet year (1993) and over the regions with increased rainfall (the central and eastern United States).

In general, the regional mean seasonal cycle of the hydrological terms were improved. Of course, precipitation was dramatically improved from Control and R-2. Moisture convergence was also improved. Evaporation correlated better with NARR (not shown). Other features of the PA hydrologic seasonal cycle

TABLE 2. Surface temperature and 2-m air temperature annual means for western, central, and eastern United States and CONUS for 1988 and 1993.

1988		PA	Control	R-2	NARR	CRU
Western	$T_{2\text{-m}}$*	282.5	282.6	281.7	283.7	283.2
Western	T_{sfc}**	282.7	282.8	281.7	284.8	
Central	$T_{2\text{-m}}$	287.0	287.2	286.0	286.4	285.9
Central	T_{sfc}	287.2	287.3	285.9	287.4	
Eastern	$T_{2\text{-m}}$	285.7	285.6	284.1	285.2	285.3
Eastern	T_{sfc}	285.8	285.6	284.0	285.8	
CONUS	$T_{2\text{-m}}$	284.6	284.8	283.6	284.9	284.6
CONUS	T_{sfc}	284.9	284.9	283.6	285.9	
1993		PA	Control	R-2	NARR	CRU
Western	$T_{2\text{-m}}$	281.6	281.6	280.7	282.6	282.1
Western	T_{sfc}	281.8	281.7	280.7	283.7	
Central	$T_{2\text{-m}}$	286.7	287.0	284.7	285.4	285.3
Central	T_{sfc}	286.8	287.1	284.6	286.0	
Eastern	$T_{2\text{-m}}$	285.9	285.9	283.9	285.3	285.4
Eastern	T_{sfc}	286.0	286.0	283.8	285.7	
CONUS	$T_{2\text{-m}}$	284.2	284.3	282.6	284.1	283.9
CONUS	T_{sfc}	284.3	284.4	282.6	284.9	

* $T_{2\text{-m}}$ = 2-m air temperature (K).
** T_{sfc} = surface temperature (K).

Unauthenticated | Downloaded 04/29/25 09:21 AM UTC

(snow, soil moisture), especially over the eastern United States, were brought closer to R-2 and NARR during the spring–summer. Finally, the reduction of the PA precipitation from Control had a significant impact on the land surface scheme runoff. The decrease in the runoff generation is related to the OSU version used by the ECPC-RSM that probably needs to be better tuned for North America. Still, the PA runoff difference features were closer to the UNH/EOS runoff fields than Control and R-2.

Overall, PA had a positive impact on the surface hydrology and energy budgets. Similarly to NARR, PA downward LW radiation flux increased, which might be related to the augmentation of the cloud cover. Although global and regional reanalyses as well as both regional simulations had larger surface SW fluxes than SRB, in comparison to Control, R-2, and NARR, PA brought the SW annual values closer to the SRB values.

The 2-m air temperature differences were also improved with respect to the CRUTEM2 differences between 1993 and 1988 in comparison to Control and R-2. Over the upper Mississippi River basin (1993 flood area), PA differences were closer to the CRUTEM2 differences than Control, suggesting that PA changes in the precipitation could also correct the near-surface temperature, which might be due to changes in the soil moisture.

The PA scheme presented here is now being changed to assimilate higher temporal resolution rain rates and to use more complex vertical structure functions to adjust the moisture profiles. These modifications will hopefully provide even more skillful simulations of the surface and atmosphere water and energy budgets, which we hope will eventually lead to more skillful monthly to seasonal predictions.

Acknowledgments. This research was funded by a cooperative agreement from NOAA-NA17RJ1231 and NASA NNG06GE64G and NNG05GR40G. The views expressed herein are those of the authors and do not necessarily reflect the views of NOAA or NASA. The GEWEX/Surface Radiation Budget (SRB) Project data were obtained from the NASA Langley Research Center Atmospheric Sciences Data Center. The NCEP/DOE AMIP-II reanalysis was obtained from the NCEP (NOMADS2) data server, and NCEP NARR monthly means were obtained online at http://www.emc.ncep.noaa.gov/mmb/rreanl. The precipitation datasets were originally obtained from the NOAA/Climate Prediction Center. CRU anomalies and absolute temperatures were obtained online at http://www.cru.uea.ac.uk/cru/data/temperature. We thank Ellen Douglas at the UNH/EOS for the runoff datasets. We would also like to thank the reviewers and the editor for their helpful comments.

REFERENCES

Aonashi, K., 1993: An initialization method to incorporate precipitation data into a mesoscale numerical weather prediction model. *J. Meteor. Soc. Japan,* **71,** 393–406.

Berbery, E. H., K. E. Mitchell, S. Benjamin, T. Smirnova, H. Ritchie, R. Hogue, and E. Radeva, 1999: Assessment of land-surface energy budgets from regional and global models. *J. Geophys. Res.,* **104** (D16), 19 329–19 348.

Betts, A. K., J. H. Ball, A. C. M. Beljaars, M. J. Miller, and P. A. Viterbo, 1996: The land surface–atmosphere interaction: A review based on observational and global modeling perspectives. *J. Geophys. Res.,* **101** (D3), 7209–7225.

Campana, K. A., Y. T. Hou, K. E. Mitchell, S. K. Yang, and R. Cullather, 1994: Improved diagnostic cloud parameterization in NMC's global model. Preprints, *10th Conf. on Numerical Weather Prediction,* Portland, OR, Amer. Meteor. Soc., 324–325.

Chou, M. D., 1992: A solar-radiation model for use in climate studies. *J. Atmos. Sci.,* **49,** 762–772.

——, and M. J. Suarez, 1994: An efficient thermal infrared radiation parameterization for use in general circulation models. Tech. Rep. Series on Global Modeling and Data Assimilation, Vol. 3, NASA Tech. Memo. 104606, 85 pp.

——, and K.-T. Lee, 1996: Parameterizations for the absorption of solar radiation by water vapor and ozone. *J. Atmos. Sci.,* **53,** 1203–1208.

Daly, C., R. P. Neilson, and D. L. Phillips, 1994: A statistical-topographic model for mapping climatological precipitation over mountainous terrain. *J. Appl. Meteor.,* **33,** 140–158.

Dirmeyer, P. A., A. J. Dolman, and N. Sato, 1999: The pilot phase of the Global Soil Wetness Project. *Bull. Amer. Meteor. Soc.,* **80,** 851–878.

Donner, L. J., 1988: An initialization for cumulus convection in numerical weather prediction models. *Mon. Wea. Rev.,* **116,** 377–385.

Falkovich, A., E. Kalnay, S. Lord, and M. B. Mathur, 2000: A new method of observed rainfall assimilation in forecast models. *J. Appl. Meteor.,* **39,** 1282–1298.

Fekete, B. M., C. J. Vörösmarty, and W. Grabs, 2002: High-resolution fields of global runoff combining observed river discharge and simulated water balances. *Global Biogeochem. Cycles,* **16,** 1042, doi:10.1029/1999GB001254.

Fillion, L., and R. Errico, 1997: Variational assimilation of precipitation data using moist convective parameterization schemes: A 1D-Var study. *Mon. Wea. Rev.,* **125,** 2917–2942.

Fu, Q., K. N. Liou, M. C. Cribb, T. P. Charlock, and A. Grossman, 1997: Multiple scattering parameterization in thermal infrared radiative transfer. *J. Atmos. Sci.,* **54,** 2799–2812.

Heckley, W. A., G. Kelly, and M. Tiedtke, 1990: On the use of satellite-derived heating rates for data assimilation within the tropics. *Mon. Wea. Rev.,* **118,** 1743–1757.

Higgins, R. W., W. Shi, E. Yarosh, and R. Joyce, 2000: *Improved U.S. Precipitation Quality Control System and Analysis.*

Unauthenticated | Downloaded 04/29/25 09:21 AM UTC

NCEP/Climate Prediction Center Atlas 7, NOAA/NWS, 40 pp.

Hou, A. Y., D. V. Ledvina, A. M. Da Silva, S. Q. Zhang, J. Joiner, R. M. Atlas, G. J. Huffman, and C. D. Kummerow, 2000: Assimilation of SSM/I-derived surface rainfall and total precipitable water for improving the GEOS analysis for climate studies. *Mon. Wea. Rev.,* **128,** 509–537.

Janjić, Z. I., 1990: The step-mountain coordinate: Physical package. *Mon. Wea. Rev.,* **118,** 1429–1443.

——, 1994: The step-mountain eta coordinate model: Further developments of the convection, viscous sublayer, and turbulence closure schemes. *Mon. Wea. Rev.,* **122,** 927–945.

Jones, P. D., and A. Moberg, 2003: Hemispheric and large-scale surface air temperature variations: An extensive revision and an update to 2001. *J. Climate,* **16,** 206–223.

Juang, H.-M. H., and M. Kanamitsu, 1994: The NMC nested regional spectral model. *Mon. Wea. Rev.,* **122,** 3–26.

Kalnay, E., and Coauthors, 1996: The NCEP/NCAR 40-Year Reanalysis Project. *Bull. Amer. Meteor. Soc.,* **77,** 437–471.

Kanamitsu, M., and K. C. Mo, 2003: Dynamical effect of land surface processes on summer precipitation over the southwestern United States. *J. Climate,* **16,** 496–509.

——, W. Ebisuzaki, J. Woollen, S.-K. Yang, J. J. Hnilo, M. Fiorino, and G. L. Potter, 2002: NCEP–DOE AMIP-II Reanalysis (R-2). *Bull. Amer. Meteor. Soc.,* **83,** 1631–1643.

Kasahara, A., A. P. Mizze, and L. J. Donner, 1994: Diabatic initialization for improvement in the tropical analysis of divergence and moisture using satellite radiometric imagery data. *Tellus,* **46A,** 242–264.

Kistler, R., and Coauthors, 2001: The NCEP–NCAR 50-Year Reanalysis: Monthly means CD-ROM and documentation. *Bull. Amer. Meteor. Soc.,* **82,** 247–267.

Krishnamurti, T. N., K. Ingles, S. Cocke, R. Pasch, and T. Kitade, 1984: Details of low latitude medium range numerical weather prediction using a global spectral model. II. Effect of orography and physical initialization. *J. Meteor. Soc. Japan,* **62,** 613–649.

——, H. S. Bedi, K. Ingles, W. Heckley, and K. Ingles, 1988: Reduction of the spinup time for evaporation and precipitation in a spectral model. *Mon. Wea. Rev.,* **116,** 907–920.

——, J. Xue, H. S. Bedi, K. Ingles, and D. Oosterhof, 1991: Physical initialization for numerical weather prediction over the tropics. *Tellus,* **43AB,** 53–81.

Lin, Y., K. E. Mitchell, E. Rogers, M. E. Baldwin, and G. J. DiMego, 1999: Test assimilations of the real-time, multisensor hourly precipitation analysis into the NCEP Eta Model. Preprints, *Eighth Conf. on Mesoscale Meteorology,* Boulder, CO, Amer. Meteor. Soc., 314–344.

Lu, C.-H., M. Kanamitsu, J. O. Roads, W. Ebisuzaki, K. E. Mitchell, and D. Lohmann, 2005: Evaluation of soil moisture in the NCEP–NCAR and NCEP–DOE global reanalyses. *J. Hydrometeor.,* **6,** 391–408.

Mahrt, L., and H. Pan, 1984: A two-layer model of soil hydrology. *Bound.-Layer Meteor.,* **29,** 1–20.

Manobianco, J., S. Koch, V. M. Karyampudi, and A. J. Negri, 1994: The impact of assimilating satellite-derived precipitation rates on numerical simulations of the ERICA IOP 4 cyclone. *Mon. Wea. Rev.,* **122,** 341–365.

Marècal, V., and J.-F. Mahfouf, 2000: Variational retrieval of temperature and humidity profiles from TRMM precipitation data. *Mon. Wea. Rev.,* **128,** 3853–3866.

Maurer, E. P., G. M. O'Donnell, D. P. Lettenmaier, and J. O. Roads, 2001: Evaluation of the land surface water budget in NCEP/NCAR and NCEP/DOE reanalyses using an off-line hydrologic model. *J. Geophys. Res.,* **106,** 17 841–17 862.

Mesinger, F., Z. I. Janjić, S. Nickovic, D. Gavrilov, and D. G. Deaven, 1988: The step-mountain coordinate: Model description and performance for cases of Alpine lee cyclogenesis and for a case of an Appalachian redevelopment. *Mon. Wea. Rev.,* **116,** 1493–1518.

——, and Coauthors, 2006: North American Regional Reanalysis. *Bull. Amer. Meteor. Soc.,* **87,** 343–360.

Mitchell, K. E., and Coauthors, 2004: The multi-institution North American Land Data Assimilation System (NLDAS): Utilizing multiple GCIP products and partners in a continental distributed hydrological modeling system. *J. Geophys. Res.,* **109,** D07S90, doi:10.1029/2003JD003823.

Moorthi, S., and M. J. Suarez, 1992: Relaxed Arakawa-Schubert. A parameterization of moist convection for general circulation models. *Mon. Wea. Rev.,* **120,** 978–1002.

Nunes, A. M. B., and S. Cocke, 2004: Implementing a physical initialization procedure in a regional spectral model: Impact on the short-range rainfall forecasting over South America. *Tellus,* **56A,** 125–140.

——, and J. O. Roads, 2005: Improving regional model simulations with precipitation assimilation. *Earth Interactions,* **9.** [Available online at http://EarthInteractions.org.]

Pan, H.-L., and L. Mahrt, 1987: Interaction between soil hydrology and boundary layer developments. *Bound.-Layer Meteor.,* **38,** 185–202.

——, and W.-S. Wu, 1994: Implementing a mass flux convective parameterization package for the NMC medium-range forecast model. Preprints, *10th Conf. on Numerical Weather Prediction,* Portland, OR, Amer. Meteor. Soc., 96–98.

Pauluis, O., and K. Emanuel, 2004: Numerical instability resulting from infrequent calculation of radiative heating. *Mon. Wea. Rev.,* **132,** 673–686.

Pinker, R. T., and I. Laszlo, 1992: Modeling surface solar irradiance for satellite applications on a global scale. *J. Appl. Meteor.,* **31,** 194–211.

Puri, K., and M. J. Miller, 1990: The use of satellite data in the specification of convective heating for diabatic initialization and moisture adjustment in numerical weather prediction. *Mon. Wea. Rev.,* **118,** 67–93.

——, and N. E. Davidson, 1992: The use of infrared satellite cloud imagery as proxy data for moisture and diabatic heating in data assimilation. *Mon. Wea. Rev.,* **120,** 2329–2341.

Roads, J., and Coauthors, 2003: GCIP water and energy budget synthesis (WEBS). *J. Geophys. Res.,* **108,** 8609, doi:10.1029/2002JD002583.

Rodell, M., and Coauthors, 2004: The global land data assimilation system. *Bull. Amer. Meteor. Soc.,* **85,** 381–394.

Slingo, J. M., 1987: The development and verification of a cloud prediction model for the ECMWF model. *Quart. J. Roy. Meteor. Soc.,* **113,** 899–927.

Stull, R. B., 1988: *An Introduction to Boundary Layer Meteorology*. Kluwer Academic, 666 pp.

Takle, E. S., and Coauthors, 1999: Project to intercompare regional climate simulations (PIRCS): Description and initial results. *J. Geophys. Res.,* **104** (D16), 19 443–19 461.

Treadon, R. E., 1996: Physical initialization in the NMC global data assimilation system. *Meteor. Atmos. Phys.,* **60,** 57–86.

Tsuyuki, T., 1997: Variational data assimilation in the tropics us-

Unauthenticated | Downloaded 04/29/25 09:21 AM UTC

ing precipitation data. Part III: Assimilation of SSM/I precipitation rates. *Mon. Wea. Rev.,* **125,** 1447–1464.

Xie, P., and P. A. Arkin, 1997: Global precipitation: A 17-year monthly analysis based on gauge observations, satellite estimates, and numerical model outputs. *Bull. Amer. Meteor. Soc.,* **78,** 2539–2558.

Yap, K.-S., 1995: Impact of Newtonian assimilation and physical initialization on the initialization and prediction by a tropical mesoscale model. *Mon. Wea. Rev.,* **123,** 833–861.

Zhao, Q., T. L. Black, and M. E. Baldwin, 1997: Implementation of the cloud prediction scheme in the Eta Model at NCEP. *Wea. Forecasting,* **12,** 697–712.

Zou, X., and Y.-H. Kuo, 1996: Rainfall assimilation through an optimal control of initial and boundary conditions in a limited-area mesoscale model. *Mon. Wea. Rev.,* **124,** 2859–2882.

Županski, D., and F. Mesinger, 1995: Four-dimensional variational assimilation of precipitation data. *Mon. Wea. Rev.,* **123,** 1112–1127.

Unauthenticated | Downloaded 04/29/25 09:21 AM UTC